

# Update of the Chiou and Youngs NGA Model for the Average Horizontal Component of Peak Ground Motion and Response Spectra

Brian S.-J. Chiou<sup>a)</sup> and Robert R. Youngs<sup>b)</sup> M.EERI

We present an update to our 2008 NGA model for predicting horizontal ground motion amplitudes caused by shallow crustal earthquakes occurring in active tectonic environments. The update is based on analysis of the greatly expanded NGA-West2 ground motion database and numerical simulations. The updated model contains minor adjustments to our 2008 functional form related to style of faulting effects, hanging wall effects, scaling with the depth to top of rupture, scaling with sediment thickness, and the inclusion of additional terms for the effects of fault dip and rupture directivity. In addition, we incorporate regional differences in far-source distance attenuation and site effects between California and other active tectonic regions. Compared to our 2008 NGA model, the predicted medians by the updated model are similar for  $M > 7$  and are lower for  $M < 5$ . The aleatory variability is larger than that obtained in our 2008 model. [DOI: 10.1193/072813EQS219M]

## INTRODUCTION

This paper presents an update to our 2008 ground motion prediction equation (GMPE; Chiou and Youngs 2008a, 2008b) for peak ground acceleration (PGA), peak ground velocity (PGV), and 5% damped pseudo-spectral acceleration (PSA). The update was based on an analysis of a greatly expanded ground motion database (Ancheta et al. 2013) and an extensive set of ground motion simulations (Donahue and Abrahamson 2014), both were provided by the Pacific Earthquake Engineering Research Center (PEER) as part of the NGA-West2 Project (Bozorgnia et al. 2014).

Preliminary evaluations of the NGA-West2 data indicated the need to include regionalization to account for regional differences in far-source distance attenuation and soil response. Because the NGA-West2 database is comprised mainly of California earthquakes, our model update was initially focused on developing a GMPE for California using primarily California data to examine the needs for adjustments of our 2008 model. In the later stage of model development, the California data were supplemented with recordings from large earthquakes occurred in other active tectonic regions to verify and refine the magnitude scaling and to provide more robust estimates of aleatory variability for larger magnitudes. Regional

---

<sup>a)</sup> Division of Research, Innovation, & System Information, California Department of Transportation, Sacramento, CA

<sup>b)</sup> AMEC Environment & Infrastructure, Inc., 180 Grand Ave., Suite 1100, Oakland, CA 94612

difference in ground motion scaling in terms of far-source distance attenuation and site effects were accounted for in the final model update.

In the following, we first describe the selection of data used in the update. We then present the changes made in this update, followed by evaluations of the updated model and comparisons to our 2008 model. Finally, we offer some guidance on model applicability. Additional technical information on model update are given in our report to PEER (Chiou and Youngs 2013).

## GROUND MOTION DATA

### DATA SELECTION

The empirical dataset used in this study was selected from the NGA-West2 empirical ground motion database (Ancheta et al. 2013). The selection criteria are the same as those used previously in Chiou and Youngs (2008a, 2008b), except for changes discussed below.

Our dataset for model update was principally restricted to free-field motions from shallow crustal earthquakes in California. Free-field data from eighteen well-recorded  $M \geq 6$  earthquakes occurred outside California were added to supplement the California dataset.

Previously, we developed the bulk of our GMPE using only data for distances of 70 km or less. This data cutoff was aimed to circumvent the unwanted consequences of sampling bias in ground motion amplitude caused by data truncation at low amplitudes and large distances (Chiou and Youngs 2008a, 2008b). In this update, instead of applying a uniform cutoff distance to all earthquakes, we assessed the maximum usable distance ( $R_{max}$ ) for each earthquake to take advantage of usable data at distances larger than 70 km. The method for assessing  $R_{max}$  is described in the subsection “Data Truncation and  $R_{max}$ .” This assessment resulted in a  $R_{max}$  shorter than 70 km for some of the older events, thus reducing the amount of data from some of the older earthquakes from that used to develop our 2008 model.

In Chiou and Youngs (2008a) we included data from aftershocks (Class 2 earthquakes as defined in Wooddell and Abrahamson 2014) to help constrain the coefficients of the site response model. With the expanded NGA-West2 database, it is no longer necessary to do so. Therefore, we excluded Class 2 earthquakes located within 20 km of a Class 1 earthquake. One notable Class 2 earthquake removed is the 1999 Duzce, Turkey, earthquake.

After applying the selections described above, a total of 12,244 records selected from 300 earthquakes were used in the update of our GMPE. Among them, a total of 2,587 records were selected from the eighteen well-recorded non-California earthquakes. Figure 1 shows a scatter plot of the distance-magnitude-region distribution of our selected dataset.

### $Z_{1.0}$ – $V_{s30}$ RELATIONSHIP

The thickness of near-surface sediments is represented in our GMPE by the depth to the shear-wave velocity horizon of 1.0 km/s,  $Z_{1.0}$ . The NGA-West2 database contains  $Z_{1.0}$  for recording sites within the Southern California Earthquake Center three-dimensional basin model, for sites within the USGS three-dimensional velocity model for the San Francisco

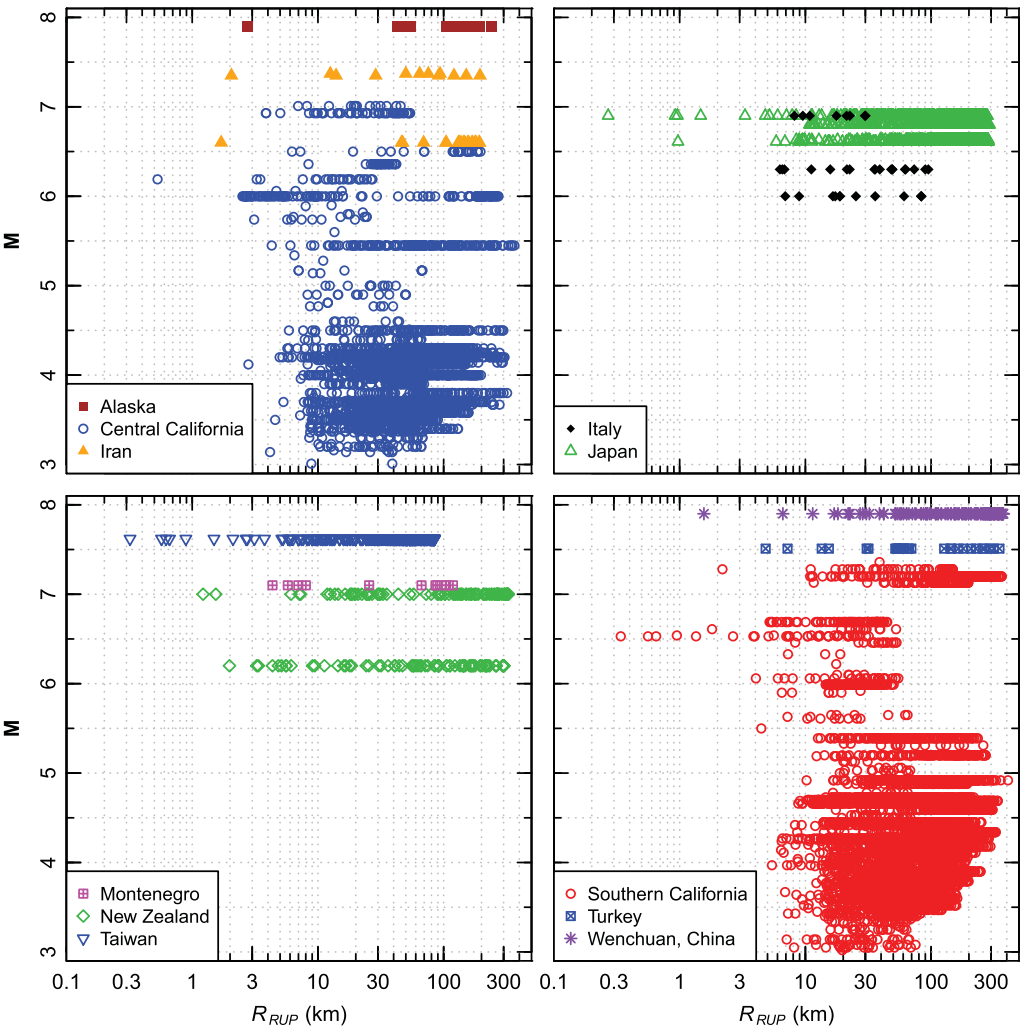


**Figure 1.** Magnitude-distance-region distribution of selected ground motion recordings used in model development.

Bay Area, for Japanese sites within the NIED (National Institute for Earth Science and Disaster Prevention) velocity model, and for sites where measured shear-wave velocity profiles reached the 1.0 km/s horizon.

As was done for our 2008 analysis, we estimated  $Z_{1.0}$  for recording stations without reported values using an updated relationship between  $Z_{1.0}$  and  $V_{S30}$  (travel-time averaged shear-wave velocity of the top 30 m of soil). Data in the NGA-West2 database show a clear difference in  $Z_{1.0}$ – $V_{S30}$  relationship between California and Japan. Therefore, we developed a separate relationship for Japan.

For California and non-Japan regions:

$$\ln(Z_{1.0}) = \frac{-7.15}{4} \ln \left( \frac{V_{S30}^4 + 571^4}{1360^4 + 571^4} \right) \quad (1)$$

For Japan:

$$\ln(Z_{1.0}) = \frac{-5.23}{2} \ln \left( \frac{V_{S30}^2 + 412^2}{1360^2 + 412^2} \right) \quad (2)$$

The units for  $Z_{1.0}$  and  $V_{S30}$  are meter and meter/second, respectively. The functional form in Equations 1 and 2 was selected to follow the trend in available  $Z_{1.0}$  and  $V_{S30}$  data.

## MODEL CHANGES

Development of the GMPE formulation used in [Chiou and Youngs \(2008a\)](#) was aimed to match the observed trends in data and to provide reasonable extrapolation outside data ranges, at the expense of moderately increased complexity in the functional form. In this update, the 2008 formulation was extensively reviewed in light of the NGA-West2 data and the set of ground motion simulations performed to evaluate hanging wall effects. The basic formulations for scaling with magnitude, distance, and  $V_{S30}$  developed for the 2008 model were found to perform satisfactorily, with changes to the pertinent model coefficients to improve fits to the expanded dataset. Formulations for scaling with style of faulting, depth to the top of rupture ( $Z_{TOR}$ ), sediment thickness ( $Z_{1.0}$ ), and hanging wall location were modified to reflect trends in data and simulation results. Two additional components were added to the GMPE to account for the effects of fault dip observed at small magnitudes and for the effects of rupture directivity at large magnitudes. Each of these changes is discussed below.

## MAGNITUDE SCALING

Development of the magnitude scaling formulation in our 2008 GMPE was guided by the results of stochastic simulations using seismological models of earthquake source spectra. Subsequent analyses by [Chiou et al. \(2010\)](#) concluded that this formulation is suitable to model magnitude scaling of PGA and PSA data of 0.3 s and 1 s over the broad magnitude range of  $M$  3 to  $M$  8, requiring only modification of a few model coefficients to remove data misfits below  $M$  5.5. We further tested its suitability for the other spectral periods ( $T$ ) against the NGA-West2 data and reached the same conclusion about the functional form. As a result, we retain the 2008 formulation for magnitude scaling but modify its coefficients  $c_3$ ,  $c_n$ , and  $c_M$  to improve the fit to the observed magnitude scaling for  $M < 5.5$  data.

## DISTANCE SCALING

In [Chiou and Youngs \(2008b\)](#) we demonstrated that a range of formulations could be used to satisfactorily model the magnitude-dependent effects of extended ruptures on distance scaling in the rupture distance ( $R_{RUP}$ ) range of 0 km to approximately 100 km. Our 2008 GMPE adopted a  $M$ - and  $T$ -independent near-source geometric spreading, coupled with a  $M$ -dependent additive distance to capture the effects of extended ruptures. This

near-source distance scaling was then gradually transitioned to a far-source geometric spreading proportion to  $R_{RUP}^{-1/2}$  in order to model the transition from body-wave geometric spreading near the source to ssurface/Lg-wave geometric spreading at larger distances. In addition, we included a  $\mathbf{M}$ - and  $T$ -dependent attenuation term,  $\gamma(\mathbf{M}, T) \times R_{RUP}$ , to capture the deviation from the above-mentioned geometric spreading due to the effects of anelastic attenuation and scattering (i.e., the effects of crustal  $Q$ ). The combined formulation was shown to satisfactorily model the attenuation of ground motion amplitudes over the distance range of 0 to several hundred kilometers for data from well recorded earthquakes. Also, it has the added advantage of providing a convenient mechanism to accommodate differences in  $Q$  among different tectonic regions. For these reasons, we continue to use the 2008 formulation for distance scaling but update the GMPE coefficients related to  $\gamma(\mathbf{M}, T)$  and account for the regional variation in  $\gamma(\mathbf{M}, T)$  observed in the NGA-West2 data.

### Data Truncation and $R_{max}$

Parameter  $\gamma$  and its magnitude dependence were assessed in this study and in [Chiou and Youngs \(2008a, 2008b\)](#) by fitting data for individual earthquakes using truncated regression (e.g., [Toro 1981](#); [Bragato 2004](#)) to account for data truncation at low amplitudes and large distances. This approach was also used in this study to estimate the distance limit  $R_{max}$  below which data distribution for that earthquake is likely to be unaffected by truncation. Figure 2 shows an example of the fit to the PGA data for two earthquakes, the 17 January 1994  $\mathbf{M}$  6.69 Northridge, California earthquake and the 31 October 2007  $\mathbf{M}$  5.45 earthquake 11 km east of Milpitas, California. The data fit was conducted using truncated regression analyses with the truncation level (defined as the second-lowest PGA data point) indicated by the horizontal dotted line. The fitted median for the average  $V_{S30}$  and  $Z_{1.0}$  of the data is plotted as the solid curve. The vertical dashed line indicates the estimated  $R_{max}$ , set at the point where the truncation level represents 2.5 standard deviations below the fitted median. The values of  $R_{max}$  estimated for each earthquake were applied to define the distance ranges for the selected earthquakes shown on Figure 1. This made it feasible for us to conduct regression analysis of the entire selected dataset using a regular mixed-effects regression method based on a non-truncated probability distribution. For a well-recorded earthquake, such as the 2007 Milpitas earthquake presented in Figure 2, the value of  $R_{max}$  is relatively large. However, for older earthquakes with high PGA truncation levels, such as the 1994 Northridge earthquake, the values of  $R_{max}$  are often less than the 70 km cutoff distance we used in developing our previous model.

### California $\gamma(\mathbf{M}, T)$

The effect of  $\mathbf{M}$  on  $\gamma$  is modeled as  $\gamma(\mathbf{M}, T) = c_{\gamma 1} + \frac{c_{\gamma 2}}{\cosh(\max[\mathbf{M}_i - c_{\gamma 3}, 0])}$ . In the 2008 GMPE, we were unable to estimate  $c_{\gamma 1}$ ,  $c_{\gamma 2}$ , and  $c_{\gamma 3}$  except for PGA. Development of the  $\gamma(\mathbf{M}, T)$  model for spectral accelerations was based on a limited dataset of just three well-recorded  $\mathbf{M}$  4.3 to 4.9 southern California earthquakes and the assumption of proportional magnitude dependence to that obtained for PGA. The large number of well-recorded California earthquakes in the NGA-West2 database allowed us to relax that assumption.

In this update, we assessed the variation of  $\gamma$  with period for three magnitude intervals. For each period and magnitude interval, a variance weighted average of the fitted values of  $\gamma$  for individual earthquakes was computed. The results shown in Figure 3 suggest that the

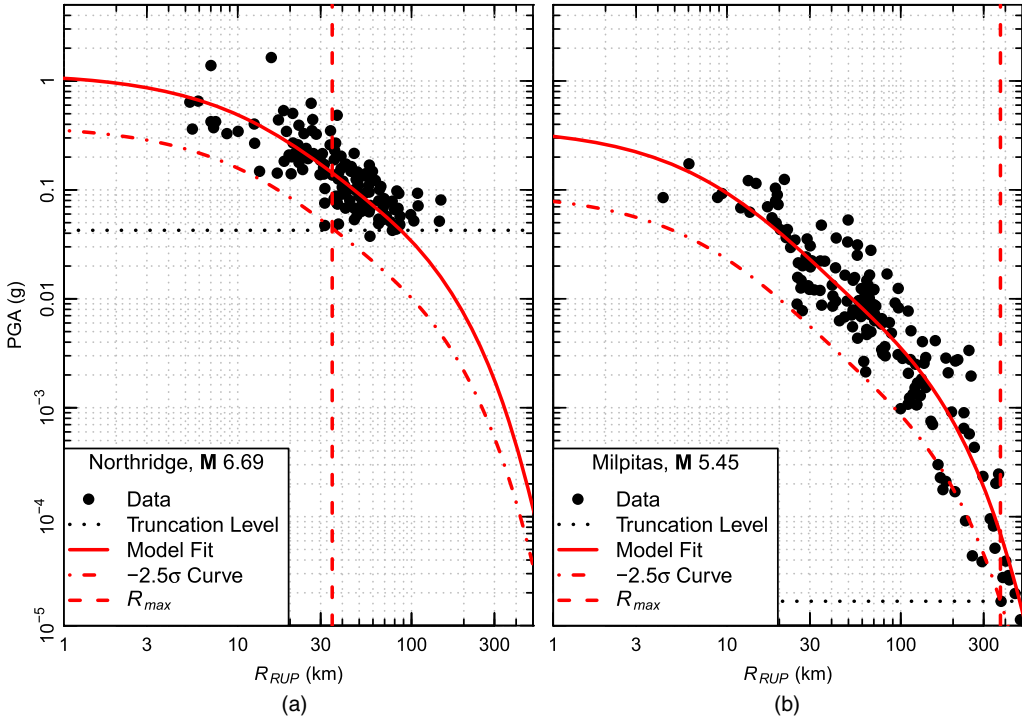


**Figure 2.** Fit of the distance scaling function form of [Chiou and Youngs \(2008\)](#) to PGA data from (a) the 17 January 1994 M 6.69 Northridge, California, earthquake and (b) the 31 October 2007 M 5.45 earthquake near Milpitas, California.

variation in  $\gamma$  with period is magnitude dependent, as opposed to the assumption of magnitude independence we used in developing our 2008 GMPE. The observed behavior is likely due to differences in the frequency content of motions contributing to peak response spectral amplitude at a given period as the magnitude of the earthquake changes. This finding prompted us to update the  $\gamma(M, T)$  model coefficients ( $c_{\gamma 1}$ ,  $c_{\gamma 2}$ , and  $c_{\gamma 3}$ ) using the combined data set shown in Figure 1.

### Regional Variation in $\gamma$

Recently, [Chiou and Youngs \(2012\)](#) found from the analysis of a worldwide dataset that there are significant regional differences in  $\gamma$  for active tectonic regions. To examine regional  $\gamma$  differences in NGA-West2 data, individual earthquake analysis was extended to earthquakes from regions outside California, including aftershocks that were not selected for use in the model update. Figure 4 shows the results of fitting the data for individual earthquakes from Italy, Japan, New Zealand, Taiwan, Turkey, and Wenchuan, China. The  $\gamma$  estimates for New Zealand, Taiwan, and Turkey are generally similar to those obtained for California earthquakes. The values for Italy and Japan indicate more rapid far-source attenuation with distance than California at most spectral periods. The data for the Wenchuan, China, earthquake and its aftershocks show slower distance attenuation. Such regional differences

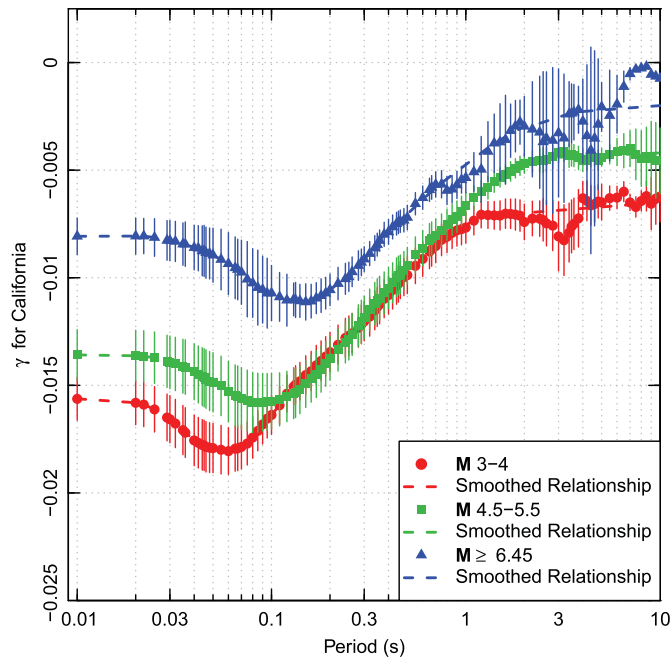


**Figure 3.** Average values of estimated  $\gamma$  for California earthquakes in three magnitude intervals obtained from fits of the distance scaling function form of Chiou and Youngs (2008) to the data for individual California earthquakes. The symbols represent variance-weighted averages of the estimated  $\gamma_s$  for individual earthquakes and the vertical lines indicate 95% confidence intervals.

were not readily apparent in our 2008 analysis due to the limited extent of data from other regions contained in the previous NGA database and the fact that those earthquakes came primarily from regions with similar attenuation characteristics (e.g., Taiwan and Turkey). In the updated GMPE, we accounted for the regional  $\gamma$  differences by applying multiplicative adjustment factors to the California  $\gamma(\mathbf{M}, T)$  model.

**Additive Distance in Near-Source Distance Scaling**

Using an initial  $\gamma(\mathbf{M}, T)$  model, we estimated for each earthquake the additive distance that controlled the near-source distance scaling. The results indicated that the estimated additive distances are generally larger than the values for our 2008 model. This finding prompted us modify coefficients  $c_5$ ,  $c_{HM}$ , and  $c_6$  as part of the model update.

**STYLE OF FAULTING AND  $Z_{TOR}$**

**Interaction with Magnitude**

In Chiou and Youngs (2008a), we did not evaluate the magnitude dependence for scaling with style of faulting and  $Z_{TOR}$ . Exploratory analysis of NGA-West2 data, however, indicated that the style-of-faulting effect is weaker for  $\mathbf{M} < 5$  earthquakes than for  $\mathbf{M} > 6$  earthquakes. Similarly, there are differences in  $Z_{TOR}$  scaling between the small and the large earthquakes,

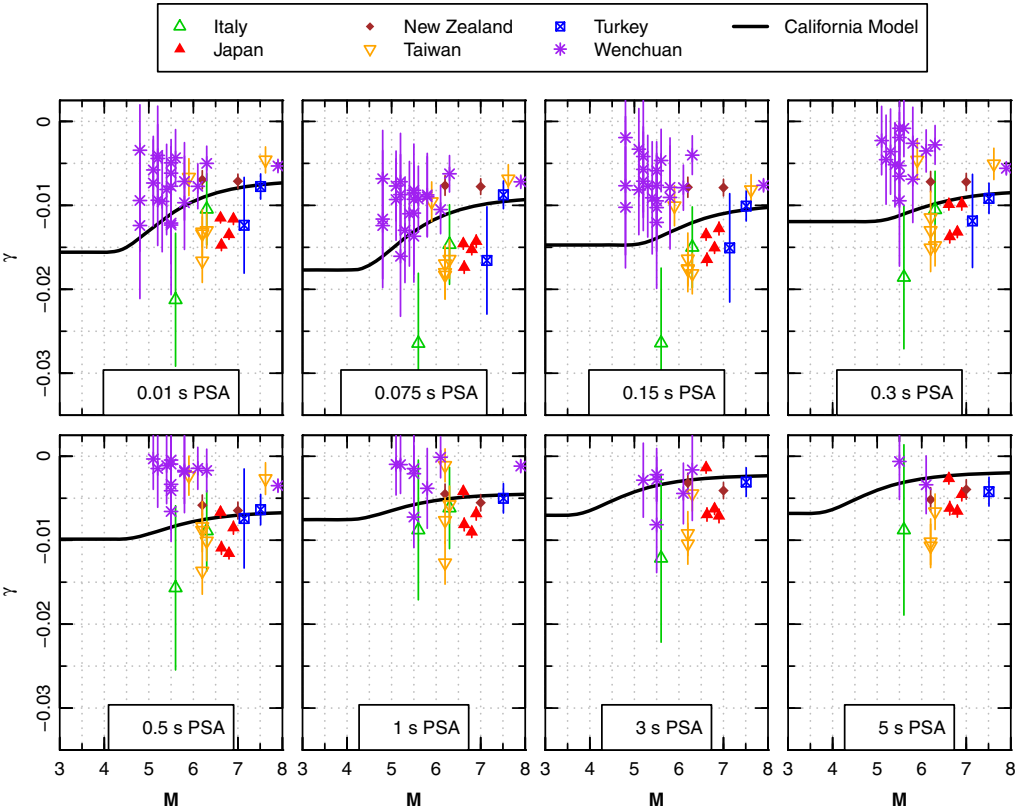


**Figure 4.** Estimates of  $\gamma$  obtained from fits to the data for individual earthquakes from various active tectonic regions other than California. The vertical line indicates the 95% confidence interval for the individual earthquake  $\gamma$  estimate.

particularly  $Z_{TOR}$  scaling is negative for  $M < 4.5$  at long periods. As a result, we introduced interaction between magnitude and these two scaling terms in the updated GMPE. The introduced magnitude interaction is given by Equation 3:

$$f(\mathbf{M}_i) = \left\{ \alpha + \frac{\beta}{\cosh[2 \cdot \max(\mathbf{M}_i - 4.5, 0)]} \right\} \tag{3}$$

Equation 3 produces a gradual change in scaling coefficient from the value  $(\alpha + \beta)$  at  $M < 4.5$  to the value  $\alpha$  at  $M > 6.5$ . Use of Equation 3 prevents undue influence on large-magnitude scaling by small earthquakes whose values of the predictors  $M$ ,  $Z_{TOR}$ , and focal mechanism have greater uncertainty than those for larger magnitudes.

**Centered  $Z_{TOR}$**

Besides the interaction with magnitude, another adjustment to  $Z_{TOR}$  scaling is the centering of  $Z_{TOR}$  on its magnitude-dependent mean, rather than on the (less meaningful)

constant mean of 4 km as in our 2008 GMPE. To implement the new centering, we developed a model relating mean  $Z_{TOR}$  to  $\mathbf{M}$ . As an alternative to the method of [Kaklamanos et al. \(2011\)](#), we applied a square root transformation to  $Z_{TOR}$  data in the NGA-West2 database to increase the normality of residuals (J. Kaklamanos, personal communication). Examination of the transformed data indicated that  $\sqrt{Z_{TOR}}$  is nearly a constant at  $\mathbf{M} < 5$  and it can be approximated by a linear  $\mathbf{M}$  function at  $\mathbf{M} > 6$ . In addition, as noted by Kaklamanos (personal communication), the  $\sqrt{Z_{TOR}} - \mathbf{M}$  relationship for reverse and reverse oblique faulting is different from the relationship for other styles of faulting. We thus developed two models, one for the reverse and reverse oblique faulting,

$$Z_{TOR} = \max[2.704 - 1.226 \max(\mathbf{M} - 5.849, 0), 0]^2 \quad (4)$$

and the other for the combined strike-slip and normal faulting,

$$Z_{TOR} = \max[2.673 - 1.136 \max(\mathbf{M} - 4.970, 0), 0]^2 \quad (5)$$

The unit for  $Z_{TOR}$  is kilometer.

Using the centered  $Z_{TOR}$ , magnitude scaling of the mean  $Z_{TOR}$  input is transferred to the general magnitude scaling of the GMPE. The effect is a sharper corner in the magnitude scaling curve compared to our 2008 model, although it has a small impact on median predictions. For convenience, we introduced the centered variable  $\Delta Z_{TOR} = Z_{TOR} - E[Z_{TOR}]$ , where  $E[Z_{TOR}]$  is the mean  $Z_{TOR}$  given by Equations 4 or 5. Depth scaling in the updated GMPE is then defined based on the value of  $\Delta Z_{TOR}$ .

## FAULT DIP EFFECT

Preliminary analysis of the NGA-West2 data indicated that event terms for  $\mathbf{M} < 5$  earthquakes increase systematically with increasing dip angle ( $\delta$ ) in a way that can be adequately modeled by  $\cos^2(\delta)$ . The same analysis indicated that the fault dip effect is insignificant for  $\mathbf{M} > 6$  earthquakes. To model dip effect, we added a  $\cos^2(\delta)$  term multiplied by Equation 3 to reflect the diminishing dip effect as  $\mathbf{M}$  increases.

## HANGING WALL EFFECT

For the evaluation of hanging wall (HW) effects, we divided the hanging wall side of ruptures into regions of  $R_{JB} = 0$  and  $R_{JB} > 0$ . For  $R_{JB} = 0$  (region inside the surface projection of the ruptured area), there is very limited data in NGA-West2 database that can be used to define the trend of HW amplification with  $R_X$ , the horizontal distance from the top of the rupture measured perpendicular to strike. Therefore, we used simulated data to develop the updated HW model for this region. The numerical simulations were conducted as part of the NGA-West2 project and are described in [Donahue and Abrahamson \(2014\)](#), along with a proposed model for HW scaling by the same authors. For  $R_{JB} > 0$  (region outside the surface projection of the ruptured area), more empirical data are available and they were used in the review of distance attenuation of HW effects.

### Sites with $R_{JB} = 0$

For the region of  $R_{JB} = 0$ , the HW amplification model presented in Donahue and Abrahamson (2013) show a more gradual rate of increase with distance  $R_X$  than predicted

by our 2008 HW formulation. This finding prompted us to revise our HW formulation according to the following analysis. The footwall data for an individual simulation were fit using a simple distance attenuation functional form. Then the residuals with respect to the fitted footwall model were computed for the simulated data at  $R_{JB} = 0$  sites. This analysis was repeated for each simulation, and the resulting sets of residuals were combined. Each plot in Figure 5 shows the residuals plotted versus  $R_X$  for a specific dip angle. The trends with  $R_X$  were interpreted as due to HW effect. With the exception of the results from the **M** 6 simulations, the simulated HW effects exhibit a similar  $R_X$  trend for all of the larger magnitudes. This trend can be reasonably modeled by the function  $\tanh(R_X/c_{9b})$ , where  $c_{9b}$  is a constant independent of magnitude. The residuals for the **M** 6 simulations exhibit a different behavior, in that they peak at very small values of  $R_X$ , rather than at values of  $R_X$  near the down dip extent of the ruptures, as is the case for the simulations from larger magnitudes. This different behavior may be the effect of the simulation process for smaller magnitudes. Because of this different behavior, the residuals for the **M** 6 simulations were not used to develop the updated hanging wall model.

The simulated HW amplifications also show a decrease in amplitude with increasing dip angle that can be modeled as a function of  $\cos(\delta)$ . The use of  $\cos(\delta)$  rather than  $\delta$  is motivated by considering the hanging wall effect to be a geometrical effect representing the location of a site relative to the projection of the entire rupture plane to the surface, with the size of this projection directly related to  $\cos(\delta)$ . The simulation residuals also show a small step at  $R_X = 0$ . Based on the above considerations, our revised HW formulation is given by Equation 6.

$$f_{HW} = c_9 \cos(\delta) \left\{ c_{9a} + (1 - c_{9a}) \tanh\left(\frac{R_X}{c_{9b}}\right) \right\} \left\{ 1 - \frac{\sqrt{R_{JB}^2 + Z_{TOR}^2}}{R_{RUP} + 1} \right\} \quad (6)$$

The fitted values of this function is compared to the residuals for  $R_{JB} = 0$  sites on Figure 5.

The revised HW model provides a stronger magnitude scaling of HW effects than our previous model, consistent with the HW model by Donahue and Abrahamson (2014). Although Equation 6 does not contain magnitude explicitly, its maximum value is higher for wider ruptures and corresponding larger magnitudes. The step in ground motions at the fault trace for surface rupturing earthquakes is also consistent with Donahue and Abrahamson (2014). However, in our formulation, this step in ground motions disappears quickly as  $Z_{TOR}$  increases from zero. The constant in the denominator of the term  $\left\{ 1 - \frac{\sqrt{R_{JB}^2 + Z_{TOR}^2}}{R_{RUP} + 1} \right\}$  was increased from 0.001 used in Chiou and Youngs (2008a) to 1 to provide a smooth decrease in HW amplification with increasing  $Z_{TOR}$ .

### Sites with $R_{JB} > 0$

For sites located beyond the edge of the rupture, the Donahue and Abrahamson (2014) model shows a less rapid attenuation of the HW amplification with increasing  $R_X$  than our 2008 formulation. For this type of site location there is more empirical data available and these data indicate a faster decay of the HW amplification with increasing  $R_X$  than is defined by the Donahue and Abrahamson (2014) hanging wall model.

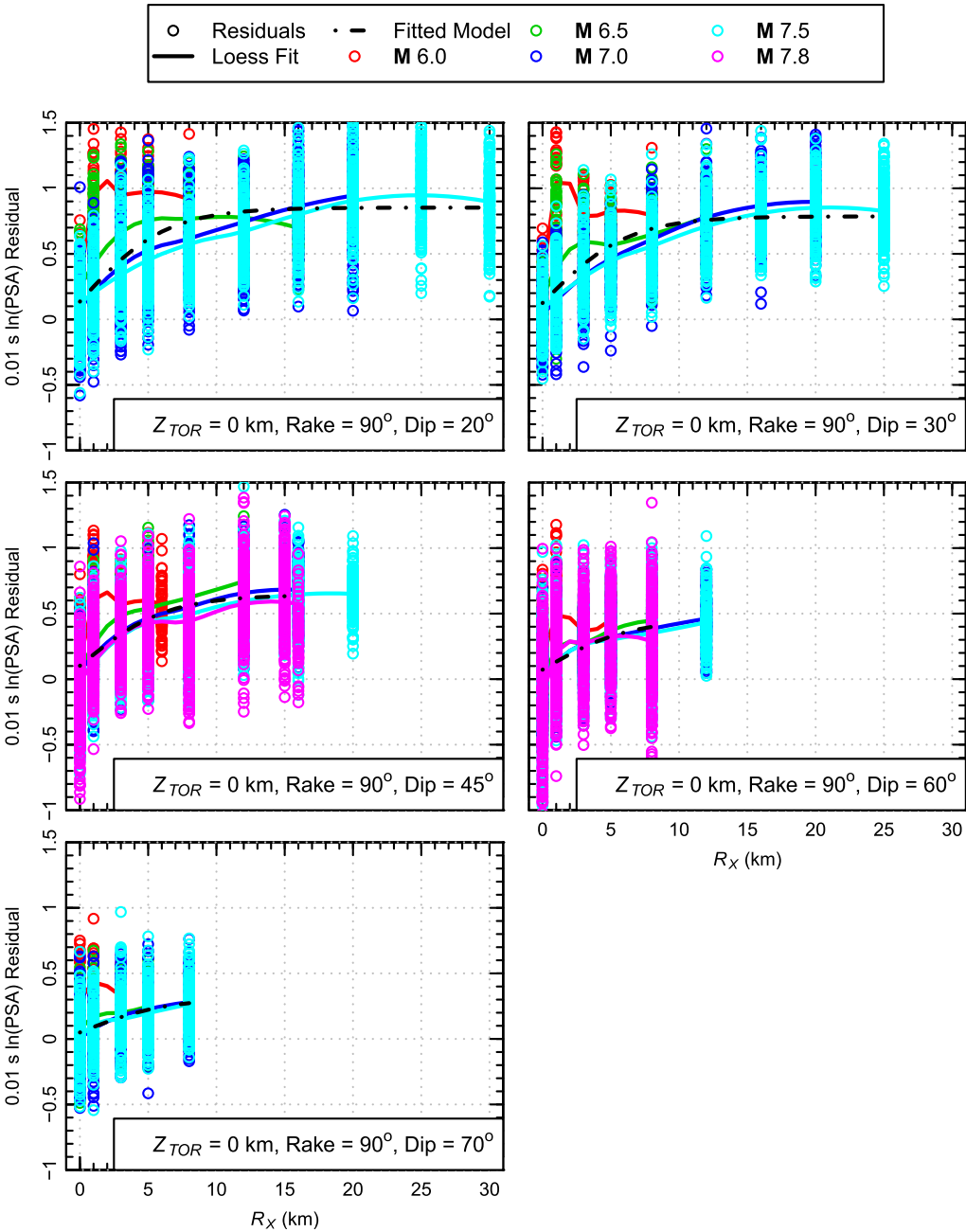


**Figure 5.** Residuals for simulated ground motion data (simulated hanging wall amplification) at sites on top of the hanging wall ( $R_{JB} = 0$ ) of reverse faulting earthquakes.

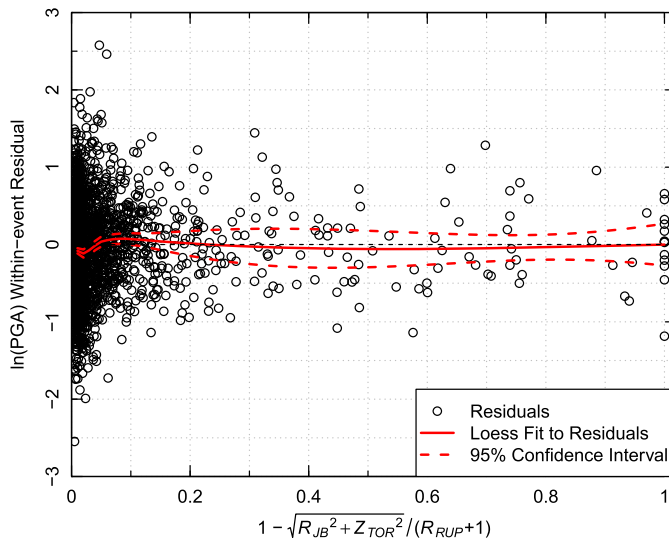


**Figure 6.** A PGA residual plot showing the adequacy of Equation 6 in modeling the distance attenuation of hanging wall effect.

To illustrate the adequacy of Equation 6 for  $R_{JB} > 0$  sites, Figure 6 compares the residuals from the updated model for sites on the hanging wall side (positive  $R_x$ ) for reverse faulting earthquakes against the distance scaling term  $\{1 - \frac{\sqrt{R_{JB}^2 + Z_{TOR}^2}}{R_{RUP} + 1}\}$ . The solid and dashed curves indicate the locally weighted least squares (loess) fit (Cleveland and others, 1992) to the residuals and the 95% confidence interval on the fit, respectively. As was found in Chiu and Youngs (2008a, 2008b), the available HW data are consistent with a linear trend in this term.

## DIRECTIVITY EFFECTS

The 2008 NGA GMPEs did not explicitly model directivity effects. Instead, they were applied as a *post facto* factor (for example, Spudich and Chiou 2008). Incorporating directivity effect as a part of the updated GMPE was one of our objectives. Among the five directivity parameterizations discussed in Spudich et al. (2013), we choose the direct point parameter (*DPP*) as our predictor of directivity effect. The rationales for choosing *DPP* over *IDP* (the isochrone directivity parameter used in Spudich and Chiou, 2008) are discussed by Chiou and Spudich (Chapter 6 of Spudich et al. 2013).

As with  $Z_{1,0}$  and  $Z_{TOR}$ , *DPP* is centered on its mean, defined as the average *DPP* value over a suite of sites located at the same distance to an earthquake. Several approaches for computing the average *DPP* were suggested by Spudich and Chiou (Chapter 5 of Spudich et al. 2013). In general, average *DPP* is a function of distance, and it is specific to the earthquake rupture being investigated. The use of centered *DPP* ( $\Delta DPP$ ) forces directivity scaling to be defined relative to the specified average *DPP*, rather than to an unknown *DPP* value embedded in the event term.

We adopted the narrow-band formulation of directivity effect proposed by Spudich and Chiou (Chapter 5 of [Spudich et al. 2013](#)) for its improved modeling of  $\mathbf{M}$  and period dependence. Their formulation was rearranged so that it could be implemented one period at a time. The rearranged form is given by Equation 7.

$$f_{DPP} = c_8 f_R f_M e^{-c_{8a}(\mathbf{M} - c_{8b})^2} \Delta DPP \quad (7)$$

Note that in the original narrow-band formulation  $c_8$  is a linear function of  $\mathbf{M}$  in the  $\mathbf{M} > 5.7$  range. We found that estimate of this linear dependence was unstable across periods and was statistically insignificant for many periods. As a result, we did not incorporate the linear magnitude dependence in the updated model. Also in the original formulation,  $c_8$  is independent of period. This property cannot be easily implemented in our one-period-at-a-time regression setting. As a workaround, we estimated  $c_8$  for each of the analyzed periods between 0.75 s and 10 s, and took the weighted average of the individual estimates as the period-independent estimate of  $c_8$ .

Function  $f_R$  in Equation 7 is the same distance taper used in [Spudich and Chiou \(2008\)](#),

$$f_R = \max \left[ 0, 1 - \frac{\max(R_{RUP} - 40, 0)}{30} \right] \quad (8)$$

Due to the absence of finite-fault information, directivity effect for  $\mathbf{M} < 5.7$  earthquakes cannot be investigated in this update. We assumed directivity effect at  $\mathbf{M} < 5.5$  is negligible, though some recent studies (for example, [Boatwright 2007](#)) suggested otherwise. This modeling assumption was implemented via the magnitude taper  $f_M$  given in Equation 9.

$$f_M = \min \left[ 1, \frac{\max(\mathbf{M} - 5.5, 0)}{0.8} \right] \quad (9)$$

This taper has the effect of reducing  $f_{DPP}$  to zero over the magnitude range from  $\mathbf{M}$  6.3 to  $\mathbf{M}$  5.5.

## $Z_{1,0}$ SCALING

Sediment thickness, represented by  $Z_{1,0}$ , was used together with  $V_{S30}$  to model the amplification of reference rock motion by local subsurface conditions. Our 2008 study found large amplification for deep sediment sites (sites where  $Z_{1,0}$  is larger than coefficient  $\phi_7$  of our 2008 GMPE). However, we were unable to observe the de-amplification predicted by site response analysis for shallow sediment sites (sites where  $Z_{1,0}$  is much smaller than  $\phi_7$ ). Guided by site response analysis, [Abrahamson and Silva \(2008\)](#) included a large de-amplification of long-period motions when a site's  $Z_{1,0}$  is well below the average  $Z_{1,0}$  for the site  $V_{S30}$ . Motivated by their work, we introduced  $\Delta Z_{1,0} = Z_{1,0} - E[Z_{1,0}|V_{S30}]$ , where  $E[Z_{1,0}|V_{S30}]$  is the average  $Z_{1,0}$  given by Equation (1) or (2). Using the centered variable  $\Delta Z_{1,0}$  as the predictor of sediment thickness effects, de-amplification for shallow sediment sites was clearly illuminated. This is illustrated in Figure 7 by the negative average value of station terms for stations with negative  $\Delta Z_{1,0}$ . The station term in the figure is defined as the average residual for recorded data available at a specific site from an interim analysis that included both linear and nonlinear  $V_{S30}$  scaling. The figure also indicates that

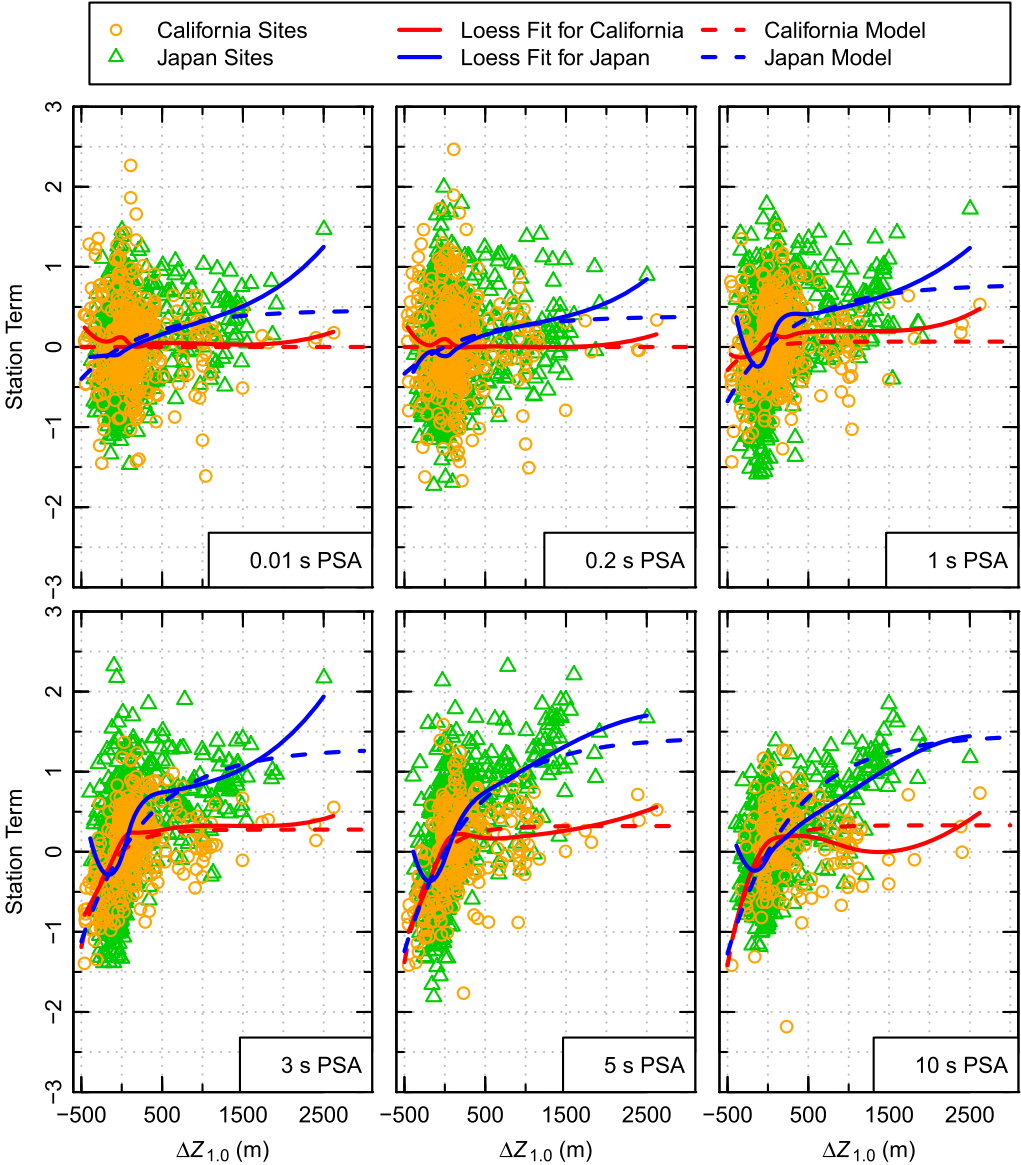


**Figure 7.** Plots showing estimated station terms versus  $\Delta Z_{1,0}$ . Stations whose  $\Delta Z_{1,0}$  were estimated using Equation 1 or 2 (hence  $\Delta Z_{1,0} = 0$ ) are not shown in this figure.

$\Delta Z_{1,0}$  scaling for positive  $\Delta Z_{1,0}$  is stronger for sites in Japan than for sites in California, indicating the need for regionalization of sediment thickness effects. Based on the trends shown on Figure 7, the revised formulation for  $Z_{1,0}$  scaling is given by Equation 10.

$$f_{Z_{1,0}} = \phi_5(1 - e^{-\Delta Z_{1,0}/\phi_6}) \tag{10}$$

### $V_{S30}$ SCALING

Our 2008 formulation for nonlinear  $V_{S30}$  scaling was found to adequately model the nonlinear soil response in NGA-West2 data. We re-estimated the linear  $V_{S30}$  scaling (coefficient  $\phi_1$ ) because there are much more weak-motion data from small-magnitude earthquakes and at large distances in the NGA-West2 database than in the previous database. The expanded weak-motion data provide a much stronger constraint on  $\phi_1$ . The revised estimates of  $\phi_1$  indicate a stronger  $V_{S30}$  linear scaling than what was obtained in our 2008 GMPE. This change is partly due to the adoption of  $\Delta Z_{1.0}$  scaling.

Chiou and Youngs (2012) noted that  $\phi_1$  for Japan is significantly different from that for California. Regional difference in  $\phi_1$  between Japan and California was also found in the NGA-West2 data. This difference was modeled in this update by a Japan-specific linear  $V_{S30}$  scaling.

### UPDATED GMPE

The revised GMPE formulation is given by Equations 11 and 12:

$$\begin{aligned}
 \ln(y_{refij}) = & c_1 + \left\{ c_{1a} + \frac{c_{1c}}{\cosh(2 \cdot \max(\mathbf{M}_i - 4.5, 0))} \right\} F_{RVi} \\
 & + \left\{ c_{1b} + \frac{c_{1d}}{\cosh(2 \cdot \max(\mathbf{M}_i - 4.5, 0))} \right\} F_{NMI} \\
 & + \left\{ c_7 + \frac{c_{7b}}{\cosh(2 \cdot \max(\mathbf{M}_i - 4.5, 0))} \right\} \Delta Z_{TORi} \\
 & + \left\{ c_{11} + \frac{c_{11b}}{\cosh(2 \cdot \max(\mathbf{M}_i - 4.5, 0))} \right\} (\cos \delta_i)^2 \\
 & + c_2(\mathbf{M}_i - 6) + \frac{c_2 - c_3}{c_n} \ln(1 + e^{c_n(c_M - \mathbf{M}_i)}) \\
 & + c_4 \ln(R_{RUPij} + c_5 \cosh(c_6 \cdot \max(\mathbf{M}_i - c_{HM}, 0))) \\
 & + (c_{4a} - c_4) \ln\left(\sqrt{R_{RUPij}^2 + c_{RB}^2}\right) \\
 & + \left\{ c_{\gamma 1} + \frac{c_{\gamma 2}}{\cosh(\max(\mathbf{M}_i - c_{\gamma 3}, 0))} \right\} R_{RUPij} \\
 & + c_8 \max\left(1 - \frac{\max(R_{RUPij} - 40, 0)}{30}, 0\right) \\
 & \times \min\left(\frac{\max(\mathbf{M}_i - 5.5, 0)}{0.8}, 1\right) e^{-c_{8a}(\mathbf{M}_i - c_{8b})^2} \Delta DPP_{ij} \\
 & + c_9 F_{HWij} \cos \delta_i \left\{ c_{9a} + (1 - c_{9a}) \tanh\left(\frac{R_{Xij}}{c_{9b}}\right) \right\} \left\{ 1 - \frac{\sqrt{R_{JBij}^2 + Z_{TORi}^2}}{R_{RUPij} + 1} \right\}
 \end{aligned} \tag{11}$$

$$\begin{aligned}
\ln(y_{ij}) = & \ln(y_{ref_{ij}}) + \eta_i \\
& + \phi_1 \cdot \min\left(\ln\left(\frac{V_{S30j}}{1130}\right), 0\right) \\
& + \phi_2(e^{\phi_3(\min(V_{S30j}, 1130)-360)} - e^{\phi_3(1130-360)}) \ln\left(\frac{y_{ref_{ij}} e^{\eta_i} + \phi_4}{\phi_4}\right) \\
& + \phi_5(1 - e^{-\Delta Z_{1.0j}/\phi_6}) \\
& + \varepsilon_{ij}
\end{aligned} \tag{12}$$

Dependent variable  $y_{ij}$  in Equation 12 is the ground motion amplitude for earthquake  $i$  at station  $j$ . Variable  $y_{ref_{ij}}$  is the population median for the reference condition  $V_{S30} = 1,130$  m/s. Random variables  $\eta_i$  (between-event residual, or event term) and  $\varepsilon_{ij}$  (within-event residual) in Equation 12 represent the two modeling errors that contribute to the aleatory variability of predicted motion. Because we excluded Class 2 earthquakes (aftershocks), we did not include aftershock terms in Equation 11. The predictor variables in Equations 11 and 12 are:

- M** = Moment magnitude.
- $R_{RUP}$  = Closest distance (km) to the ruptured plane.
- $R_{JB}$  = Closest distance (km) to the surface projection of ruptured plane.
- $R_X$  = Site coordinate (km) measured perpendicular to the fault strike from the fault line, with the down-dip direction being positive.
- $F_{HW}$  = Hanging-wall flag: 1 for  $R_X \geq 0$  and 0 for  $R_X < 0$ .
- $\delta$  = Fault dip angle.
- $Z_{TOR}$  = Depth (km) to the top of ruptured plane.
- $\Delta Z_{TOR}$  =  $Z_{TOR}$  centered on the **M**-dependent average  $Z_{TOR}$  (km).
- $F_{RV}$  = Reverse-faulting flag: 1 for  $30^\circ \leq \lambda \leq 150^\circ$  (combined reverse and reverse-oblique), 0 otherwise;  $\lambda$  is the rake angle.
- $F_{NM}$  = Normal faulting flag: 1 for  $-120^\circ \leq \lambda \leq -60^\circ$  (excludes normal-oblique), 0 otherwise.
- $V_{S30}$  = Travel-time averaged shear-wave velocity (m/s) of the top 30 m of soil.
- $Z_{1.0}$  = Depth (m) to shear-wave velocity of 1.0 km/s.
- $\Delta Z_{1.0}$  =  $Z_{1.0}$  centered on the  $V_{S30}$ -dependent average  $Z_{1.0}$  (m).
- $DPP$  = Direct point parameter for directivity effect.
- $\Delta DPP$  =  $DPP$  centered on the site- and earthquake-specific average  $DPP$ .

We used the same range of rake angles to define reverse and normal faulting flags as was used for our 2008 GMPE. The normal-faulting effects were not well constrained as our dataset for model update contains only eight **M** < 5.9 normal faulting earthquakes in California and three **M**  $\geq 6$  normal earthquakes in Italy. As a result, we did not update the normal faulting coefficients from the 2008 values. Coefficients  $c_9$ ,  $c_{9a}$ , and  $c_{9b}$  were constrained by numerical simulations, not by empirical data. GMPE coefficients (variable names starting with the letter  $c$  or  $\phi$ ) are listed in Tables 1 to 3. In the table headings, we underlined coefficients whose values were unmodified from the 2008 GMPE and we used boldface on those that were added or given a different meaning in the updated GMPE. Our modified

**Table 1.** Period-independent coefficients of model for  $\ln(y)$  (Equation 11)

<u><math>c_2</math></u>	<u><math>c_4</math></u>	<u><math>c_{4a}</math></u>	<u><math>c_{RB}</math></u>	<b><math>c_{8a}</math></b>	<b><math>c_{11}</math></b>
1.06	−2.1	−0.5	50	0.2695	0

In table heading, the underlined coefficients are those that were unmodified in values from our 2008 GMPE and the boldface coefficients are those that were added or given a different meaning in the updated GMPE.

coefficients were developed through an iterative process of performing regression for the entire set of periods with some part of the model fixed, developing smoothing models with period for a few coefficients, and then repeating the regression analysis with the smoothed coefficients fixed to their smoothed values to examine the variation of the remaining coefficients. As was done in our 2008 GMPE to correct for the sample bias in long-period PSA, we smoothed the estimated  $c_1$  values by imposing a smooth variation in the slope of  $c_1$  with respect to period. This process led to a reduction in  $c_1$  values for long periods.

To simplify, Equations 11 and 12 were written for California, although our regression analysis included regionalization to account for the observed regional difference in far-source distance attenuation and site effects. The region-specific coefficients for site effects and region-specific adjustment factors for  $\gamma(\mathbf{M}, T)$  are given in Table 4. Also, in application to sites in Japan, the Japan-specific average  $Z_{1.0}$  model given by Equation 2 was used to center  $Z_{1.0}$ .

### ALEATORY VARIABILITY

The formulations for aleatory variability developed in Chiou and Youngs (2008a) include dependence on magnitude and degree of nonlinear soil response. In this study, we updated the coefficients of the variance model to reflect the changes brought upon by the expanded NGA-West2 data and the updated median.

The current symbology for components of variability (Al Atik et al. 2010) uses the symbol  $\tau$  for the between-event component and the symbol  $\phi$  for the within-event component, with the symbol  $\sigma$  used for total aleatory variability, such that  $\sigma^2 = \tau^2 + \phi^2$ . However, to avoid confusion with our use of the symbol  $\phi$  for the coefficients of site amplification model, we retain the symbols used in Chiou and Youngs (2008a):  $\tau$  for the between-event component,  $\sigma$  for within-event component, with the symbol  $\sigma_T$  used for the total aleatory variability.

Two earthquakes, the 2000 **M** 6.61 Tottori, Japan, earthquake and the 1999 **M** 7.6 Chi-Chi, Taiwan, earthquake, have large absolute event terms compared to the rest of the larger earthquakes. Given that the sample size of large earthquakes is not large, the event terms for these two earthquakes have an impact on the assessment of  $\tau$ . Exploratory analysis of the distribution of event terms using robust regression indicated that the large event term from Tottori may be an outlier in the set of event terms. Therefore, the residuals from Tottori were removed from the assessment of  $\tau$ . The exploratory analysis using robust regression indicated that removal of the data from Chi-Chi might lead to an underestimate of  $\tau$  and hence the data from this earthquake were retained.

Table 2. Period-dependent coefficients of model for  $\ln(y_{ref})$  (Equation 11)

Period (s)	$c_1$	$c_{1a}$	$\frac{c_{1b}}{c_{1a}}$	$c_{1c}$	$c_{1d}$	$c_n$	$c_M$	$c_3$	$c_5$	$c_{HM}$	$c_6$
PGA	-1.5065	0.1650	-0.2550	-0.1650	0.2550	16.0875	4.9993	1.9636	6.4551	3.0956	0.4908
PGV	2.3549	0.1650	-0.0626	-0.1650	0.0626	3.3024	5.4230	2.3152	5.8096	3.0514	0.4407
0.01	-1.5065	0.1650	-0.2550	-0.1650	0.2550	16.0875	4.9993	1.9636	6.4551	3.0956	0.4908
0.02	-1.4798	0.1650	-0.2550	-0.1650	0.2550	15.7118	4.9993	1.9636	6.4551	3.0963	0.4925
0.03	-1.2972	0.1650	-0.2550	-0.1650	0.2550	15.8819	4.9993	1.9636	6.4551	3.0974	0.4992
0.04	-1.1007	0.1650	-0.2550	-0.1650	0.2550	16.4556	4.9993	1.9636	6.4551	3.0988	0.5037
0.05	-0.9292	0.1650	-0.2550	-0.1650	0.2550	17.6453	4.9993	1.9636	6.4551	3.1011	0.5048
0.075	-0.6580	0.1650	-0.2540	-0.1650	0.2540	20.1772	5.0031	1.9636	6.4551	3.1094	0.5048
0.1	-0.5613	0.1650	-0.2530	-0.1650	0.2530	19.9992	5.0172	1.9636	6.8305	3.2381	0.5048
0.12	-0.5342	0.1650	-0.2520	-0.1650	0.2520	18.7106	5.0315	1.9795	7.1333	3.3407	0.5048
0.15	-0.5462	0.1650	-0.2500	-0.1650	0.2500	16.6246	5.0547	2.0362	7.3621	3.4300	0.5045
0.17	-0.5858	0.1650	-0.2480	-0.1650	0.2480	15.3709	5.0704	2.0823	7.4365	3.4688	0.5036
0.2	-0.6798	0.1650	-0.2449	-0.1650	0.2449	13.7012	5.0939	2.1521	7.4972	3.5146	0.5016
0.25	-0.8663	0.1650	-0.2382	-0.1650	0.2382	11.2667	5.1315	2.2574	7.5416	3.5746	0.4971
0.3	-1.0514	0.1650	-0.2313	-0.1650	0.2313	9.1908	5.1670	2.3440	7.5600	3.6232	0.4919
0.4	-1.3794	0.1650	-0.2146	-0.1650	0.2146	6.5459	5.2317	2.4709	7.5735	3.6945	0.4807
0.5	-1.6508	0.1650	-0.1972	-0.1650	0.1972	5.2305	5.2893	2.5567	7.5778	3.7401	0.4707
0.75	-2.1511	0.1650	-0.1620	-0.1650	0.1620	3.7896	5.4109	2.6812	7.5808	3.7941	0.4575
1	-2.5365	0.1650	-0.1400	-0.1650	0.1400	3.3024	5.5106	2.7474	7.5814	3.8144	0.4522
1.5	-3.0686	0.1650	-0.1184	-0.1650	0.1184	2.8498	5.6705	2.8161	7.5817	3.8284	0.4501
2	-3.4148	0.1645	-0.1100	-0.1645	0.1100	2.5417	5.7981	2.8514	7.5818	3.8330	0.4500
3	-3.9013	0.1168	-0.1040	-0.1168	0.1040	2.1488	5.9983	2.8875	7.5818	3.8361	0.4500
4	-4.2466	0.0732	-0.1020	-0.0732	0.1020	1.8957	6.1552	2.9058	7.5818	3.8369	0.4500
5	-4.5143	0.0484	-0.1010	-0.0484	0.1010	1.7228	6.2856	2.9169	7.5818	3.8376	0.4500
7.5	-5.0009	0.0220	-0.1010	-0.0220	0.1010	1.5737	6.5428	2.9320	7.5818	3.8380	0.4500
10	-5.3461	0.0124	-0.1000	-0.0124	0.1000	1.5265	6.7415	2.9396	7.5818	3.8380	0.4500

Period (s)	$c_7$	$c_{7b}$	$c_8$	$c_{8b}$	$c_9$	$c_{9a}$	$c_{9b}$	$c_{11b}$	$c_{g1}$	$c_{g2}$	$c_{g3}$
PGA	0.0352	0.0462	0.0000	0.4833	0.9228	0.1202	6.8607	-0.4536	-0.007146	-0.006758	4.2542
PGV	0.0324	0.0097	0.2154	5.000	0.3079	0.1000	6.5000	-0.3834	-0.001852	-0.007403	4.3439
0.01	0.0352	0.0462	0.0000	0.4833	0.9228	0.1202	6.8607	-0.4536	-0.007146	-0.006758	4.2542
0.02	0.0352	0.0472	0.0000	1.2144	0.9296	0.1217	6.8697	-0.4536	-0.007249	-0.006758	4.2386
0.03	0.0352	0.0533	0.0000	1.6421	0.9396	0.1194	6.9113	-0.4536	-0.007869	-0.006758	4.2519
0.04	0.0352	0.0596	0.0000	1.9456	0.9661	0.1166	7.0271	-0.4536	-0.008316	-0.006758	4.2960
0.05	0.0352	0.0639	0.0000	2.1810	0.9794	0.1176	7.0959	-0.4536	-0.008743	-0.006758	4.3578
0.075	0.0352	0.0630	0.0000	2.6087	1.0260	0.1171	7.3298	-0.4536	-0.009537	-0.006190	4.5455
0.1	0.0352	0.0532	0.0000	2.9122	1.0177	0.1146	7.2588	-0.4536	-0.009830	-0.005332	4.7603
0.12	0.0352	0.0452	0.0000	3.1045	1.0008	0.1128	7.2372	-0.4536	-0.009913	-0.004732	4.8963
0.15	0.0352	0.0345	0.0000	3.3399	0.9801	0.1106	7.2109	-0.4536	-0.009896	-0.003806	5.0644
0.17	0.0352	0.0283	0.0000	3.4719	0.9652	0.1150	7.2491	-0.4536	-0.009787	-0.003280	5.1371
0.2	0.0352	0.0202	0.0000	3.6434	0.9459	0.1208	7.2988	-0.4440	-0.009505	-0.002690	5.1880
0.25	0.0352	0.0090	0.0000	3.8787	0.9196	0.1208	7.3691	-0.3539	-0.008918	-0.002128	5.2164
0.3	0.0352	-0.0004	0.0000	4.0711	0.8829	0.1175	6.8789	-0.2688	-0.008251	-0.001812	5.1954
0.4	0.0352	-0.0155	0.0000	4.3745	0.8302	0.1060	6.5334	-0.1793	-0.007267	-0.001274	5.0899
0.5	0.0352	-0.0278	0.0991	4.6099	0.7884	0.1061	6.5260	-0.1428	-0.006492	-0.001074	4.7854
0.75	0.0352	-0.0477	0.1982	5.0376	0.6754	0.1000	6.5000	-0.1138	-0.005147	-0.001115	4.3304
1	0.0352	-0.0559	0.2154	5.3411	0.6196	0.1000	6.5000	-0.1062	-0.004277	-0.001197	4.1667
1.5	0.0352	-0.0630	0.2154	5.7688	0.5101	0.1000	6.5000	-0.1020	-0.002979	-0.001675	4.0029
2	0.0352	-0.0665	0.2154	6.0723	0.3917	0.1000	6.5000	-0.1009	-0.002301	-0.002349	3.8949
3	0.0160	-0.0516	0.2154	6.5000	0.1244	0.1000	6.5000	-0.1003	-0.001344	-0.003306	3.7928
4	0.0062	-0.0448	0.2154	6.8035	0.0086	0.1000	6.5000	-0.1001	-0.001084	-0.003566	3.7443
5	0.0029	-0.0424	0.2154	7.0389	0.0000	0.1000	6.5000	-0.1001	-0.001010	-0.003640	3.7090
7.5	0.0007	-0.0348	0.2154	7.4666	0.0000	0.1000	6.5000	-0.1000	-0.000964	-0.003686	3.6632
10	0.0003	-0.0253	0.2154	7.7700	0.0000	0.1000	6.5000	-0.1000	-0.000950	-0.003700	3.6230

Units are g for PGA and PSA, and cm/s for PGV; PGA is taken as the same as 0.01 s PSA.

In table heading, the underlined coefficient is that which was unmodified in values from our 2008 GMPE and the boldface coefficients are those that were added or given a different meaning in the updated GMPE.

**Table 3.** Coefficients of site response model for  $\ln(y)$  (Equation 12)

Period (s)	$\Phi_1$	$\Phi_2$	$\Phi_3$	$\Phi_4$	$\Phi_5$	$\Phi_6$
PGA	−0.5210	−0.1417	−0.007010	0.102151	0.0000	300
PGV	−0.7936	−0.0699	−0.008444	5.410000	0.0202	300
0.01	−0.5210	−0.1417	−0.007010	0.102151	0.0000	300
0.02	−0.5055	−0.1364	−0.007279	0.108360	0.0000	300
0.03	−0.4368	−0.1403	−0.007354	0.119888	0.0000	300
0.04	−0.3752	−0.1591	−0.006977	0.133641	0.0000	300
0.05	−0.3469	−0.1862	−0.006467	0.148927	0.0000	300
0.075	−0.3747	−0.2538	−0.005734	0.190596	0.0000	300
0.1	−0.4440	−0.2943	−0.005604	0.230662	0.0000	300
0.12	−0.4895	−0.3077	−0.005696	0.253169	0.0000	300
0.15	−0.5477	−0.3113	−0.005845	0.266468	0.0000	300
0.17	−0.5922	−0.3062	−0.005959	0.265060	0.0000	300
0.2	−0.6693	−0.2927	−0.006141	0.255253	0.0000	300
0.25	−0.7766	−0.2662	−0.006439	0.231541	0.0000	300
0.3	−0.8501	−0.2405	−0.006704	0.207277	0.0010	300
0.4	−0.9431	−0.1975	−0.007125	0.165464	0.0040	300
0.5	−1.0044	−0.1633	−0.007435	0.133828	0.0100	300
0.75	−1.0602	−0.1028	−0.008120	0.085153	0.0340	300
1	−1.0941	−0.0699	−0.008444	0.058595	0.0670	300
1.5	−1.1142	−0.0425	−0.007707	0.031787	0.1430	300
2	−1.1154	−0.0302	−0.004792	0.019716	0.2030	300
3	−1.1081	−0.0129	−0.001828	0.009643	0.2770	300
4	−1.0603	−0.0016	−0.001523	0.005379	0.3090	300
5	−0.9872	0.0000	−0.001440	0.003223	0.3210	300
7.5	−0.8274	0.0000	−0.001369	0.001134	0.3290	300
10	−0.7053	0.0000	−0.001361	0.000515	0.3300	300

In table heading, the underlined coefficients are those that were unmodified in values from our 2008 GMPE and the boldface coefficients are those that were added or given a different meaning in the updated GMPE.

Estimates of  $\tau$  and  $\sigma$  for data in 0.5-unit magnitude intervals were calculated and used to explore the effects of various variables on aleatory variability. The primary effect observed was a general decrease in both components of aleatory variability with increasing magnitude, consistent with the findings from our 2008 model. Overall, the estimated values of  $\tau$  and  $\sigma$  indicate magnitude dependence at most periods. Therefore, the tri-linear form used in our previous model was retained. Some experimentation indicated that the appropriate magnitude break points were at **M** 5 and **M** 6.5. However, at short periods, the estimated  $\sigma$  displayed a marked increase for magnitudes less than **M** 5. Therefore, our assessment of within-event variability allowed for a discontinuity in  $\sigma$  at **M** 5. The estimated values of  $\tau$  did not show a jump in value at **M** 5. Exploratory evaluations indicated that inclusion of data from earthquakes with less than five recordings inflated the estimates of  $\tau$ , at least for smaller magnitude earthquakes. As event terms are not well constrained for earthquakes with a very limited number of recordings, the variance model parameters were estimated using data from earthquakes with at least five recordings.

**Table 4.** Model coefficients for non-California regions

Period (s)	$\gamma_{Jp-It}$	$\gamma_{Wn}$	$\Phi_{1Jp}$	$\Phi_{5Jp}$	$\Phi_{6Jp}$
PGA	1.5817	0.7594	−0.6846	0.4590	800
PGV	2.2306	0.3350	−0.7966	0.9488	800
0.01	1.5817	0.7594	−0.6846	0.4590	800
0.02	1.5740	0.7606	−0.6681	0.4580	800
0.03	1.5544	0.7642	−0.6314	0.4620	800
0.04	1.5502	0.7676	−0.5855	0.4530	800
0.05	1.5391	0.7739	−0.5457	0.4360	800
0.075	1.4804	0.7956	−0.4685	0.3830	800
0.1	1.4094	0.7932	−0.4985	0.3750	800
0.12	1.3682	0.7768	−0.5603	0.3770	800
0.15	1.3241	0.7437	−0.6451	0.3790	800
0.17	1.3071	0.7219	−0.6981	0.3800	800
0.2	1.2931	0.6922	−0.7653	0.3840	800
0.25	1.3150	0.6579	−0.8469	0.3930	800
0.3	1.3514	0.6362	−0.8999	0.4080	800
0.4	1.4051	0.6049	−0.9618	0.4620	800
0.5	1.4402	0.5507	−0.9945	0.5240	800
0.75	1.5280	0.3582	−1.0225	0.6580	800
1	1.6523	0.2003	−1.0002	0.7800	800
1.5	1.8872	0.0356	−0.9245	0.9600	800
2	2.1348	0.0000	−0.8626	1.1100	800
3	3.5752	0.0000	−0.7882	1.2910	800
4	3.8646	0.0000	−0.7195	1.3870	800
5	3.7292	0.0000	−0.6560	1.4330	800
7.5	2.3763	0.0000	−0.5202	1.4600	800
10	1.7679	0.0000	−0.4068	1.4640	800

$g_{Jp-It}$ : Multiplicative adjustment factor to California  $\gamma(\mathbf{M}, T) = c_{\gamma 1} + \frac{c_{\gamma 2}}{\cosh(\max[\mathbf{M}_I - c_{\gamma 3}, 0])}$  for Japanese and Italian data. Note that since the Japanese and Italian events used in our update are of  $6.0 < \mathbf{M} < 6.9$ , this factor is defined only for that  $\mathbf{M}$  range.

$g_{Wn}$ : Multiplicative adjustment factor to California  $\gamma(\mathbf{M}, T)$  for the  $\mathbf{M}$  7.9 2008 Wenchuan earthquake data.

$f_{1Jp}$ :  $f_1$  for Japanese data.

$f_{5Jp}$ :  $f_5$  for Japanese data.

$f_{6Jp}$ :  $f_6$  for Japanese data.

In table heading, the boldface coefficients are those that were added or given a different meaning in the updated GMPE.

Examination of the between-event residuals initially suggested dependence on distance. However, it was found that for the residuals at periods less than 1.0 s, the observed distance dependence could be largely explained by accounting for the nonlinear soil effect on site amplification and increased within-event variability for the Japanese data. The observed distance dependence at longer periods may be in fact the result of un-modeled basin effects in data from regions without estimates of  $Z_{1,0}$ , as larger estimates of  $\sigma$  were obtained for data from regions outside of California and Japan where basin velocity models are unavailable for estimating  $Z_{1,0}$ .

The estimated between-event variability for larger-magnitude earthquakes shows a sharp peak near 0.1 s period. A possible explanation is the interaction of varying stress drop with the high-frequency damping term ( $\kappa$ ) typical of sites in active tectonic regions. Experimentation using point source stochastic simulations indicated that variation of stress drop alone for a constant value of  $\kappa$  does not produce a peak in between-event variability near 0.1 s, but including both variability in stress drop among the simulated earthquakes and variability in  $\kappa$  among the different sites does introduce a peak, but the peak is in the within-event component of variability. However, if the variability in  $\kappa$  is such that each earthquake has a different average value of  $\kappa$ , then this will introduce a peak in the between-event variability. Examination of between-event variability in data from more homogeneous regions like central or southern California showed little or no peak near 0.1 s period. These results suggest the usefulness of including a term for site  $\kappa$  in future ground motion models. We attribute the peak in event-to-event variation to be the result of event-to-event differences in average site effects. This interpretation was strengthened by analysis of the small and moderate magnitude California data using a cross-classified mixed-effects model incorporating both random effects for individual events and random effects for individual sites. This analysis resulted in a peak in site-to-site variability near 10 Hz, rather than a peak in event-to-event variability. For our updated model we smoothed through the peak in event-to-event variability within the range of statistical uncertainty in estimating the event-to-event variability. The peak in site-to-site variability should be considered as an epistemic uncertainty in application of the model to an individual site.

The total variance,  $\sigma_T^2$ , for forward prediction of ground motion is given by Equation 13:

$$\begin{aligned}\sigma_T^2 &= (1 + NL_0)^2 \tau^2 + \sigma_{NL_0}^2 \\ \tau &= \tau_1 + \frac{\tau_2 - \tau_1}{1.5} (\min(\max(\mathbf{M}, 5), 6.5) - 5) \\ \sigma_{NL_0} &= \left( \sigma_1 + \frac{\sigma_2 - \sigma_1}{1.5} (\min(\max(\mathbf{M}, 5), 6.5) - 5) \right) \times \sqrt{\sigma_3 F_{inferred} + 0.7 F_{measured} + (1 + NL_0)^2} \\ NL_0 &= \phi_2 (e^{\phi_3 (\min(V_{S30}, 1130) - 360)} - e^{\phi_3 (1130 - 360)}) \left( \frac{y_{ref}}{y_{ref} + \phi_4} \right)\end{aligned}\tag{13}$$

Equation 13 implements the approximate method of Chiou and Youngs (2008a) to account for added prediction variability due to the random  $\eta_i$  effect on soil nonlinear response. The coefficients  $\phi_2$  and  $\phi_3$  are those in Equation 12 and their values are listed in Table 3. Because we excluded data from Class 2 earthquakes (aftershocks), we did not include  $\sigma_4$  (increase in  $\sigma$  for Class 2 earthquakes). The values of coefficients  $\tau_1$ ,  $\tau_2$ ,  $\sigma_1$ ,  $\sigma_2$ , and  $\sigma_3$  are listed in Table 5, along with the Japan-specific estimates of  $\sigma_2$ .

## EVALUATION OF UPDATED MODEL

Figure 8 shows the event term  $\eta_i$  (between-event residual) for spectral periods of 0.01 s (PGA), 0.2 s, 1 s, and 3 s. In the range of  $3.5 \leq \mathbf{M} \leq 8$ , the event terms do not exhibit a significant trend with  $\mathbf{M}$  or a large offset from zero. The updated

**Table 5.** Coefficients of aleatory variability model (Equation 13)

Period (s)	$\tau_1$	$\tau_2$	$\sigma_1$	$\sigma_2$	<u><math>\sigma_3</math></u>	<b><math>\sigma_{2Ip}</math></b>
PGA	0.4000	0.2600	0.4912	0.3762	0.8000	0.4528
PGV	0.3894	0.2578	0.4785	0.3629	0.7504	0.3918
0.01	0.4000	0.2600	0.4912	0.3762	0.8000	0.4528
0.02	0.4026	0.2637	0.4904	0.3762	0.8000	0.4551
0.03	0.4063	0.2689	0.4988	0.3849	0.8000	0.4571
0.04	0.4095	0.2736	0.5049	0.3910	0.8000	0.4642
0.05	0.4124	0.2777	0.5096	0.3957	0.8000	0.4716
0.075	0.4179	0.2855	0.5179	0.4043	0.8000	0.5022
0.1	0.4219	0.2913	0.5236	0.4104	0.8000	0.5230
0.12	0.4244	0.2949	0.5270	0.4143	0.8000	0.5278
0.15	0.4275	0.2993	0.5308	0.4191	0.8000	0.5304
0.17	0.4292	0.3017	0.5328	0.4217	0.8000	0.5310
0.2	0.4313	0.3047	0.5351	0.4252	0.8000	0.5312
0.25	0.4341	0.3087	0.5377	0.4299	0.7999	0.5309
0.3	0.4363	0.3119	0.5395	0.4338	0.7997	0.5307
0.4	0.4396	0.3165	0.5422	0.4399	0.7988	0.5310
0.5	0.4419	0.3199	0.5433	0.4446	0.7966	0.5313
0.75	0.4459	0.3255	0.5294	0.4533	0.7792	0.5309
1	0.4484	0.3291	0.5105	0.4594	0.7504	0.5302
1.5	0.4515	0.3335	0.4783	0.4680	0.7136	0.5276
2	0.4534	0.3363	0.4681	0.4681	0.7035	0.5167
3	0.4558	0.3398	0.4617	0.4617	0.7006	0.4917
4	0.4574	0.3419	0.4571	0.4571	0.7001	0.4682
5	0.4584	0.3435	0.4535	0.4535	0.7000	0.4517
7.5	0.4601	0.3459	0.4471	0.4471	0.7000	0.4167
10	0.4612	0.3474	0.4426	0.4426	0.7000	0.3755

In table heading, the underlined coefficients are those that were unmodified in values from our 2008 GMPE and the boldface coefficients are those that were added or given a different meaning in the updated GMPE.

model has the tendency to under predict  $T = 3$  s data in the range of  $M < 3.5$ , as evidenced by the positive event terms. There are outliers at large magnitudes, exhibiting large ( $> 2\tau$ ) absolute event terms at different periods. These are the 1999  $M$  7.6 Chi-Chi earthquake (for 0.01 s and 0.2 s PSA), the 2000  $M$  6.6 Tottori earthquake (for 0.01 s, 0.2 s, and 3 s PSA), and the 2008  $M$  7.9 Wenchuan, China, earthquake (for 1 s and 3 s PSA). All three earthquakes occurred outside California. Also shown on Figure 8 are loess fits to the event terms for just the California earthquakes and for the combined dataset, the latter plotted for just  $M \geq 6$  for clarity as only California earthquakes make up the dataset for  $M < 6$ . The 95% confident intervals for these fits encompass zero indicating no significant departures from the model. In addition, the trends for just California earthquakes are consistent with the estimates from the combined dataset at  $M > 7$ , which is dominated by non-California earthquakes.

Figures 9 through 12 show the within-event residuals  $\varepsilon_{ij}$  plotted versus  $M$ ,  $R_{RUP}$ ,  $V_{S30}$ , and  $\Delta Z_{1.0}$  for spectral periods of 0.01 s (PGA), 0.2 s, 1 s, and 3 s, respectively. In

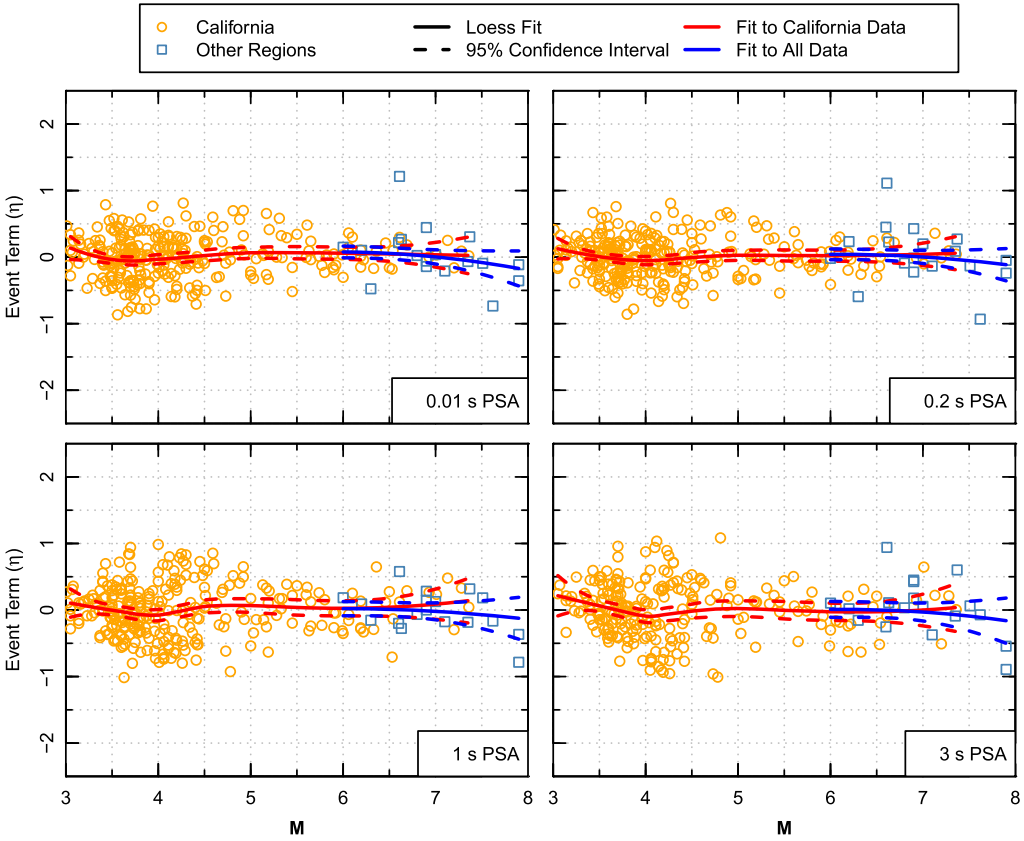


**Figure 8.** Between-event residuals (event terms) for spectral periods of 0.01 s (PGA), 0.2 s, 1 s, and 3 s.

general, these residuals do not exhibit a significant trend within the body of a predictor, but some show trends near the ends of predictor domain. We assumed there is no site amplification relative to  $y_{ref}$  for sites with  $V_{S30}$  greater than 1,130 m/s. A limited number of such high  $V_{S30}$  sites are in the NGA-West2 database, and their residuals, if anything, show a slight downward trend for 0.01 s and 0.2 s, and an upward trend for 3 s. Similar to Figure 8, loess fits to the with-event residuals for just California data and fits for the combined dataset are shown in each panel. These comparisons indicate that the trends observed for the combined data are consistent with those observed in the California data.

The adequacy of our model to represent the nonlinear soil effects in NGA-West2 data is illustrated in Figure 13. Data points shown in the figure are the within-event residuals for 0.2 s PSA computed without the effects of  $V_{S30}$  (i.e., for a  $V_{S30}$  of 1,130 m/s). These residuals can be loosely interpreted as empirical soil amplification factors (EAF) relative to the event-specific median reference motion ( $y_{ref} \exp(\eta)$ ). The EAFs are grouped by the level of reference motion and plotted against  $V_{S30}$  to show how their  $V_{S30}$  scaling varies with the level

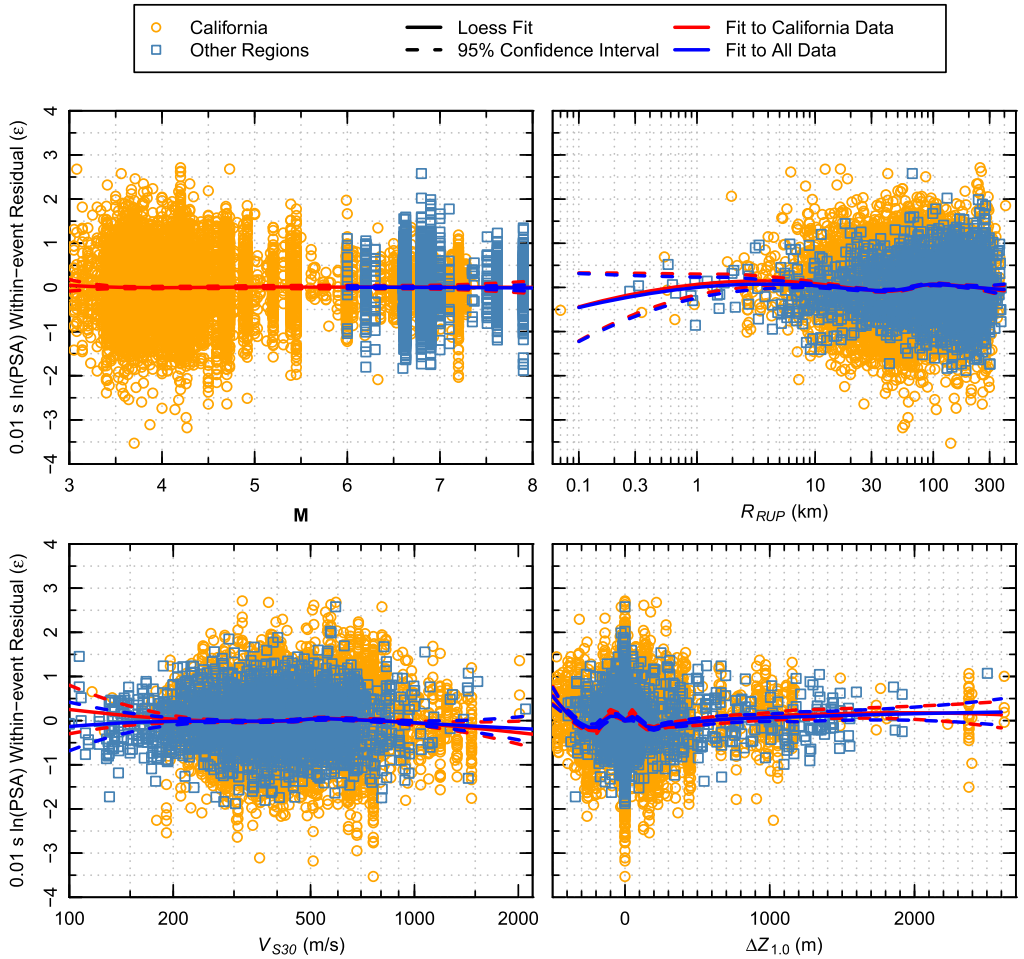


**Figure 9.** Within-event residuals for spectral period of 0.01 s (PGA) plotted against  $M$ ,  $R_{RUP}$ ,  $V_{S30}$ , and  $\Delta Z_{1.0}$ .

of reference motion. Soil amplification predicted by our updated model is also shown in the figure as the thick dot-dash curve. The good agreement between the predicted and the empirical amplifications confirms the general validity of our nonlinear soil response model. At  $V_{S30} < 200$  m/s, our model over estimates the empirical amplification of Japanese data in almost all levels of reference motion, suggesting either a deviation from linear  $\ln(V_{S30})$  scaling over the lower  $V_{S30}$  range or a stronger nonlinearity in Japanese soft soil data than what is predicted by our model.

## COMPARISON WITH CHIOU AND YOUNGS (2008)

Figure 14 compares the predicted median motions for vertical strike-slip earthquakes,  $V_{S30} = 760$  m/s, and  $\Delta DPP = 0$ . For predictions by the updated model (CY2014), we

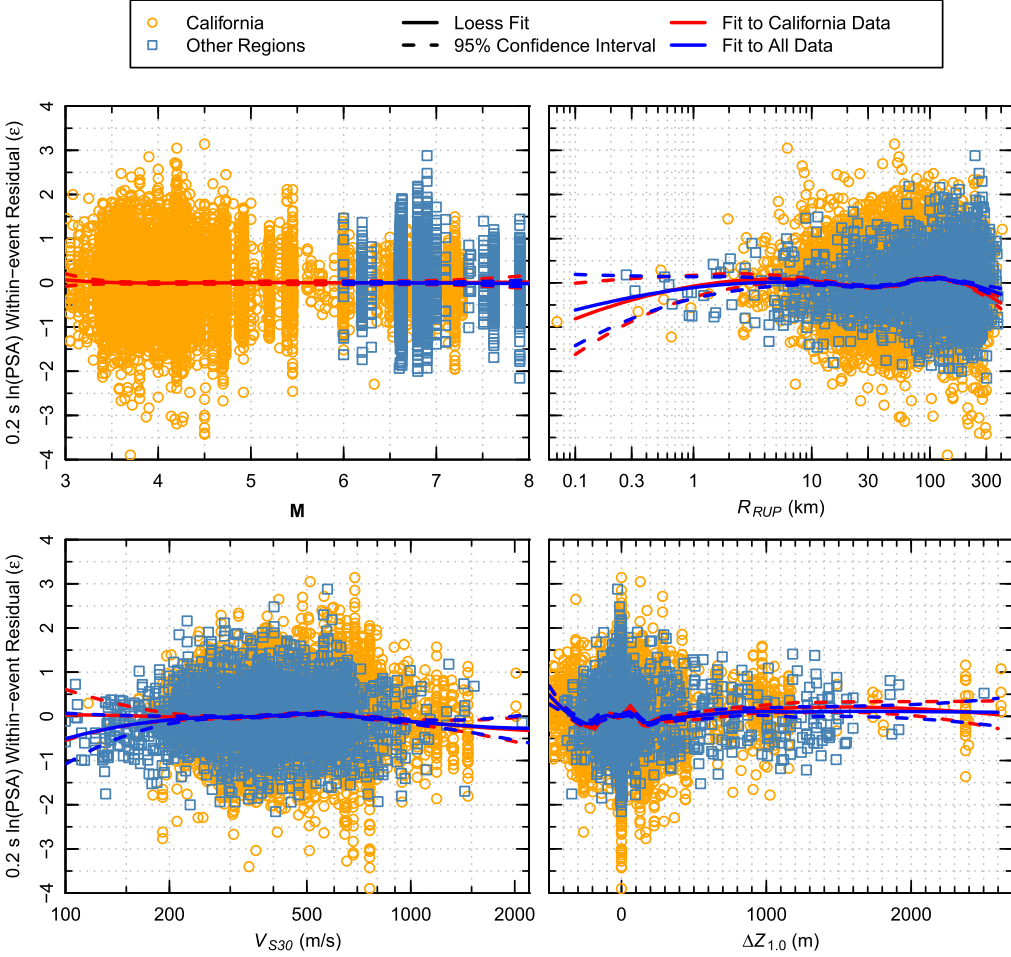


**Figure 10.** Within-event residuals for spectral period of 0.2 s plotted against  $M$ ,  $R_{RUP}$ ,  $V_{S30}$ , and  $\Delta Z_{1.0}$ .

set  $\Delta Z_{TOR}$  and  $\Delta Z_{1.0}$  to 0. Equivalently, for predictions by the 2008 GMPE (CY2008), we used average  $Z_{TOR}$  and the average  $Z_{1.0}$  based on the relationships presented above. As discussed, many of the model changes affect primarily ground motion prediction for  $M < 5.5$  earthquakes. As a result, the larger differences in predictions occur mostly at  $M < 5.5$ . For  $M > 6.0$  and  $R_{RUP} < 100$  km, the differences are typically less than 20 percent.

Figure 15 compares predicted median motions on the hanging wall side of  $45^\circ$  dipping reverse earthquakes. The predicted HW motions by CY2014 are in general smaller than those predicted by CY2008, primarily because CY2014 has a smaller HW amplification. CY2014 also has a stronger  $M$  scaling in HW amplification than CY2008 does.

Figures 16 and 17 compare predicted median response spectra for  $V_{S30} = 760$  m/s and 310 m/s, respectively. CY2014 produces similar spectral shapes to CY2008.

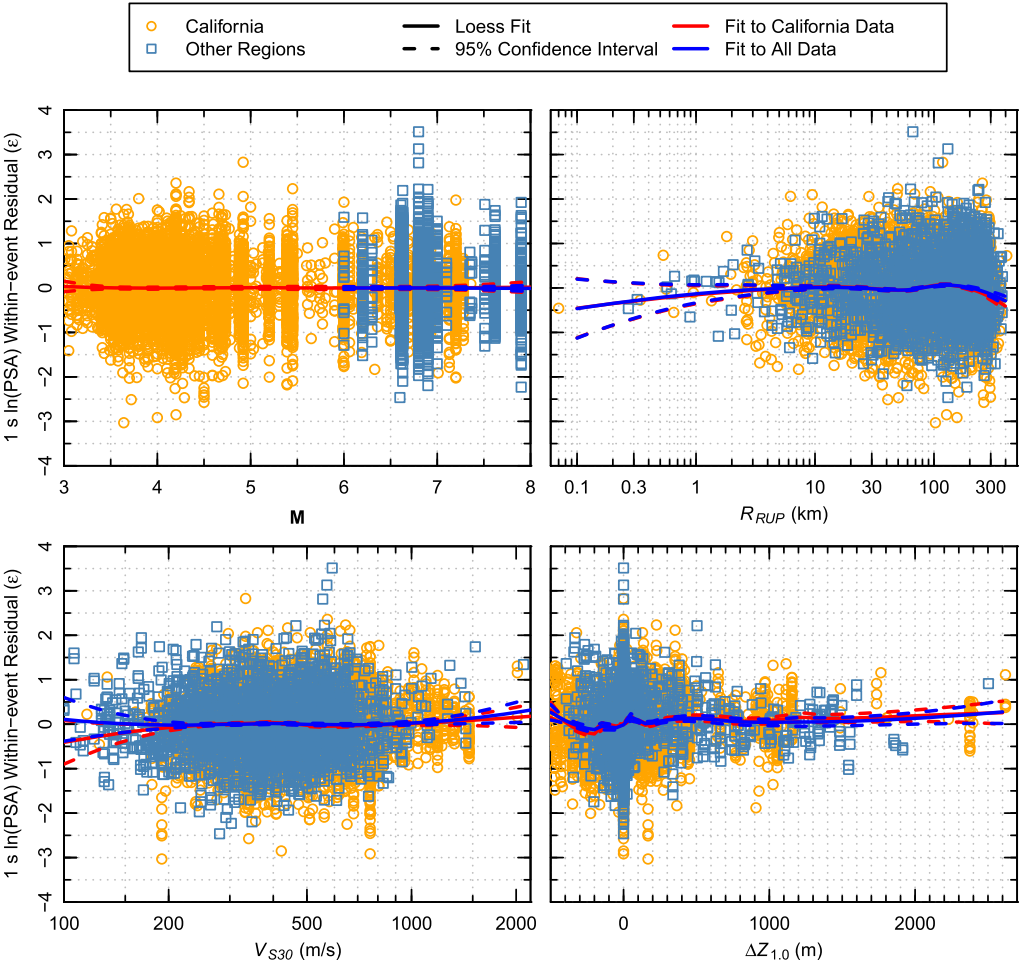


**Figure 11.** Within-event residuals for spectral period of 1 s plotted against  $M$ ,  $R_{RUP}$ ,  $V_{S30}$ , and  $\Delta Z_{1,0}$ .

### MODEL APPLICABILITY

For forward application, the median predicted amplitude is given by Equations 11 and 12 with  $\eta_i = 0$ , and the total variance  $\sigma_T$  is given by Equation 13. The updated GMPE developed in this study is considered to be applicable for predicting horizontal ground motion amplitudes for earthquakes in active tectonic regions in which the following conditions apply:

- $3.5 \leq M \leq 8.5$  for strike-slip earthquakes.
- $3.5 \leq M \leq 8.0$  for reverse and normal faulting earthquakes.
- $Z_{TOR} \leq 20$  km.
- $0 \text{ km} \leq R_{RUP} \leq 300$  km.
- $180 \text{ m/s} \leq V_{S30} \leq 1,500 \text{ m/s}$ .

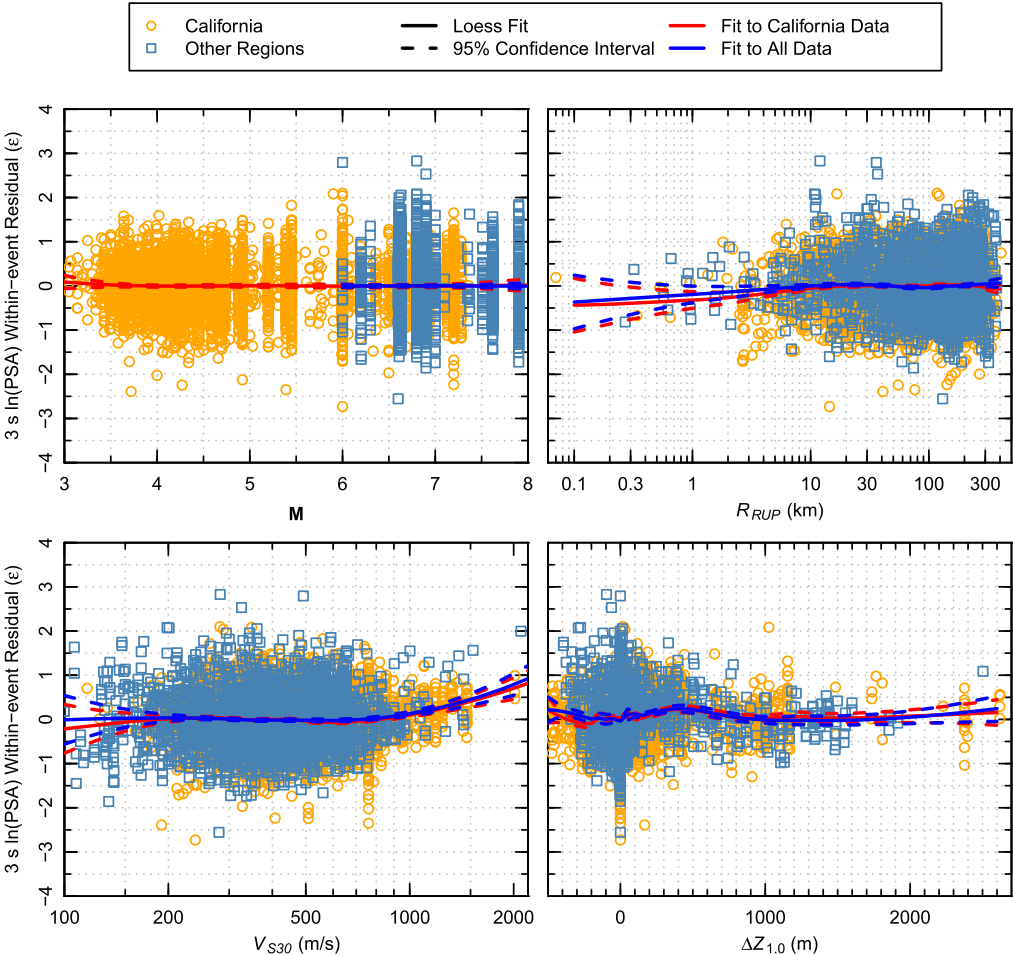


**Figure 12.** Within-event residuals for spectral period of 3 s plotted against  $M$ ,  $R_{RUP}$ ,  $V_{S30}$ , and  $\Delta Z_{1.0}$ .

Compared to [Chiou and Youngs \(2008a\)](#), the lower bound of the applicable magnitude range was lowered to  $M$  3.5 because of the large number of small earthquakes used in this update. However, because all  $M < 6$  earthquakes were from California, our GMPE may not be applicable to  $M < 6$  earthquakes in other active tectonic regions.

We increase the upper bound of the applicable distance range from 200 km to 300 km because of the use of extensive data at distances between 200 km and 300 km ([Figure 1](#)). Predicted PSA value at  $T \leq 0.3$  s should be set equal to the value of PGA when it falls below the predicted PGA, which could occur at any distance, but is an egregious error mainly at distances larger than 250 km. For application in other active tectonic regions where earthquakes at distances greater than about 50 km are a major contributor to the hazard,

adjustments to the  $\gamma(\mathbf{M}, T)$  model may be warranted. These adjustments can be made using the hybrid approach developed by Campbell (2003). In making such adjustments, we stress the need for the user to obtain estimates of  $Q$  for the two regions that are based on geometric spreading models consistent with the one used in this study.

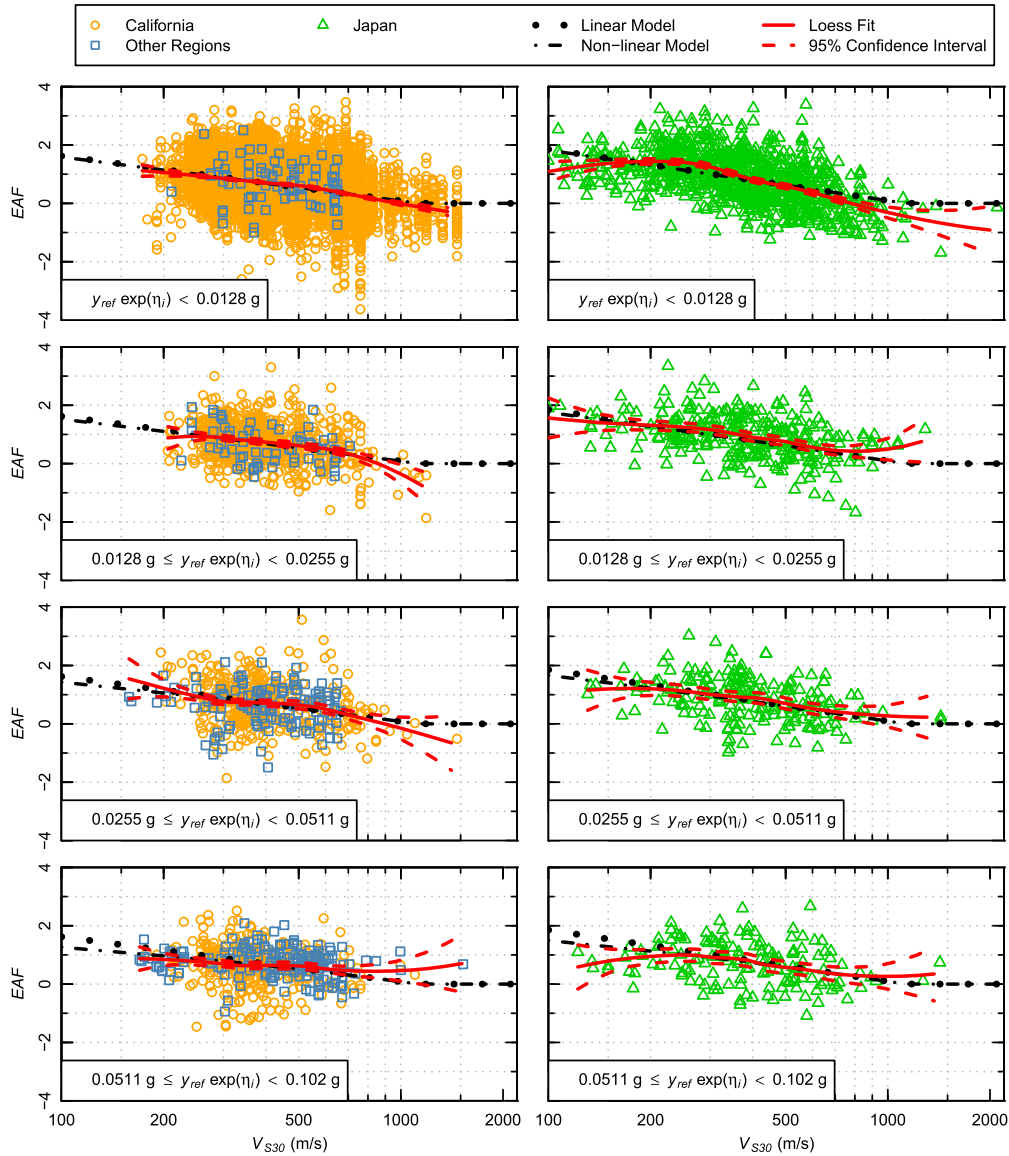


**Figure 13.** Empirical soil amplification factor ( $EAF$ ) for 0.2 s period plotted versus  $V_{S30}$  for various ranges of event-specific median reference motion ( $y_{ref} \exp(\eta_i)$ ). Each range of  $y_{ref} \exp(\eta_i)$  is shown at the lower left corner of a plot.

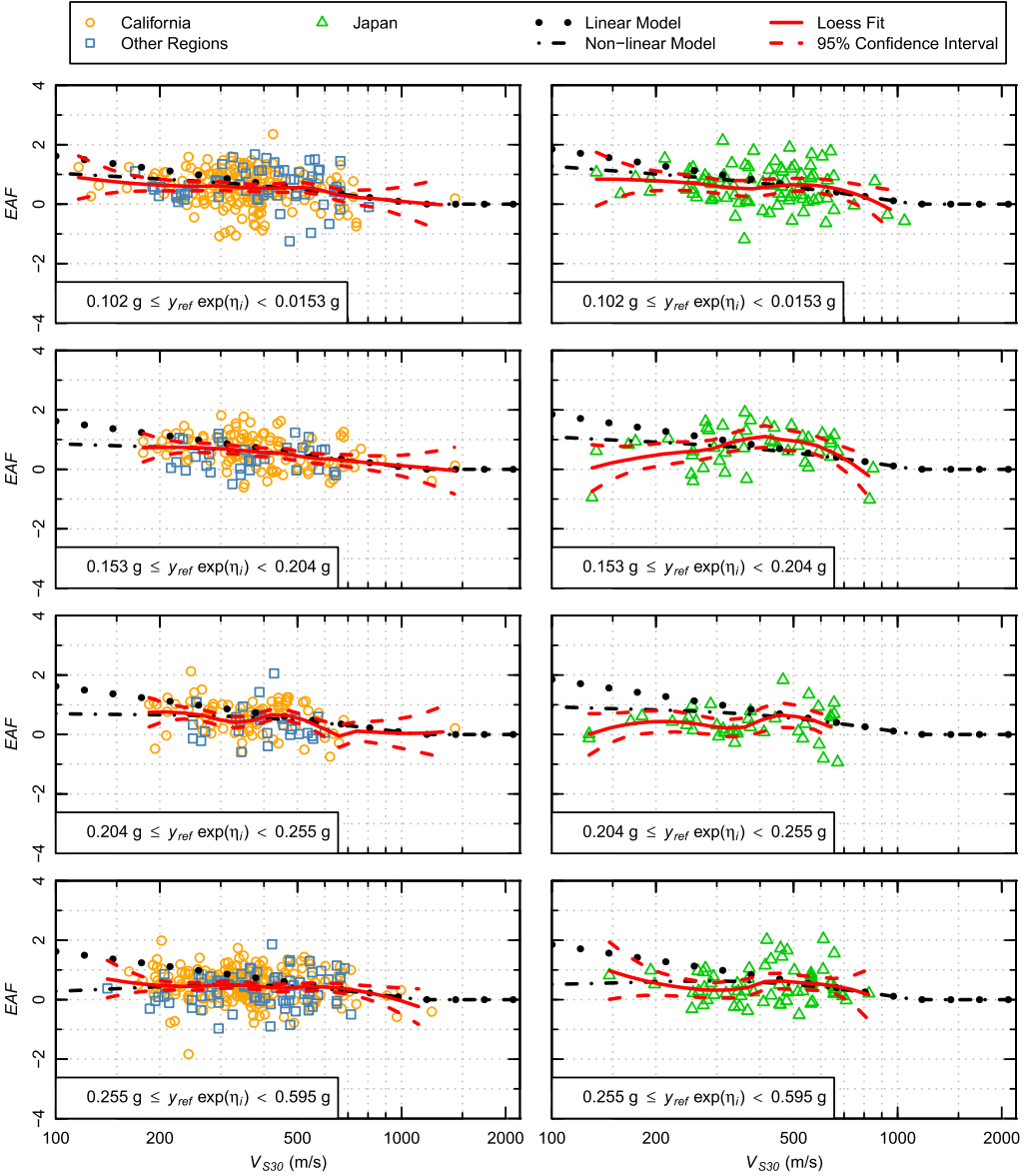


Figure 13. Continued.

We raised the lower bound of the  $V_{S30}$  applicable range from 150 m/s to 180 m/s because of the misfits observed at low  $V_{S30}$ . The site response model was constrained such that all ground motion amplification factors are 1 for  $V_{S30}$  greater than 1,130 m/s. As the rock velocity increases we expect shallow crustal damping (i.e.,  $\kappa$ ) to decrease, resulting in increases in high-frequency motion. Data for such sites were not sampled in the

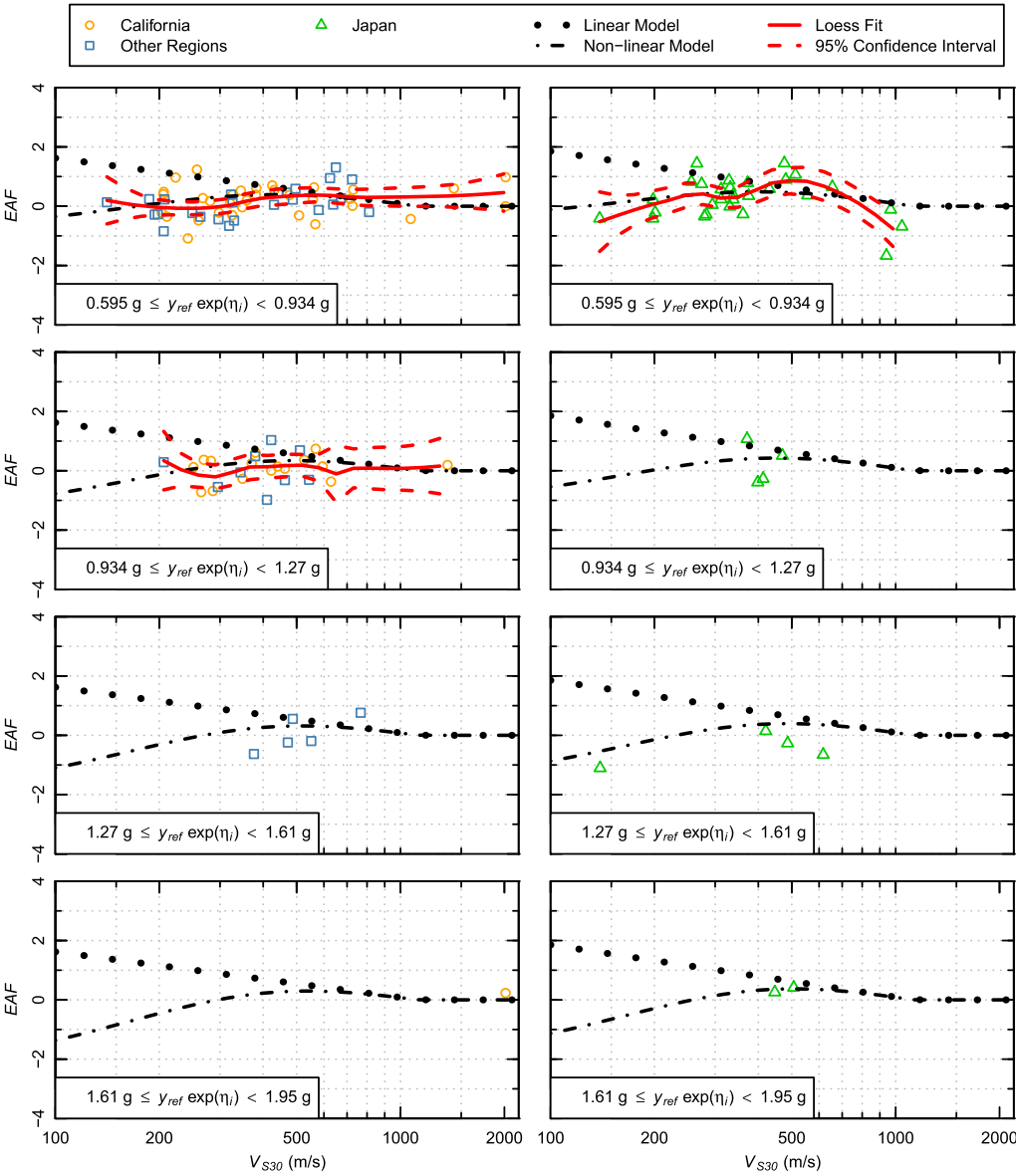
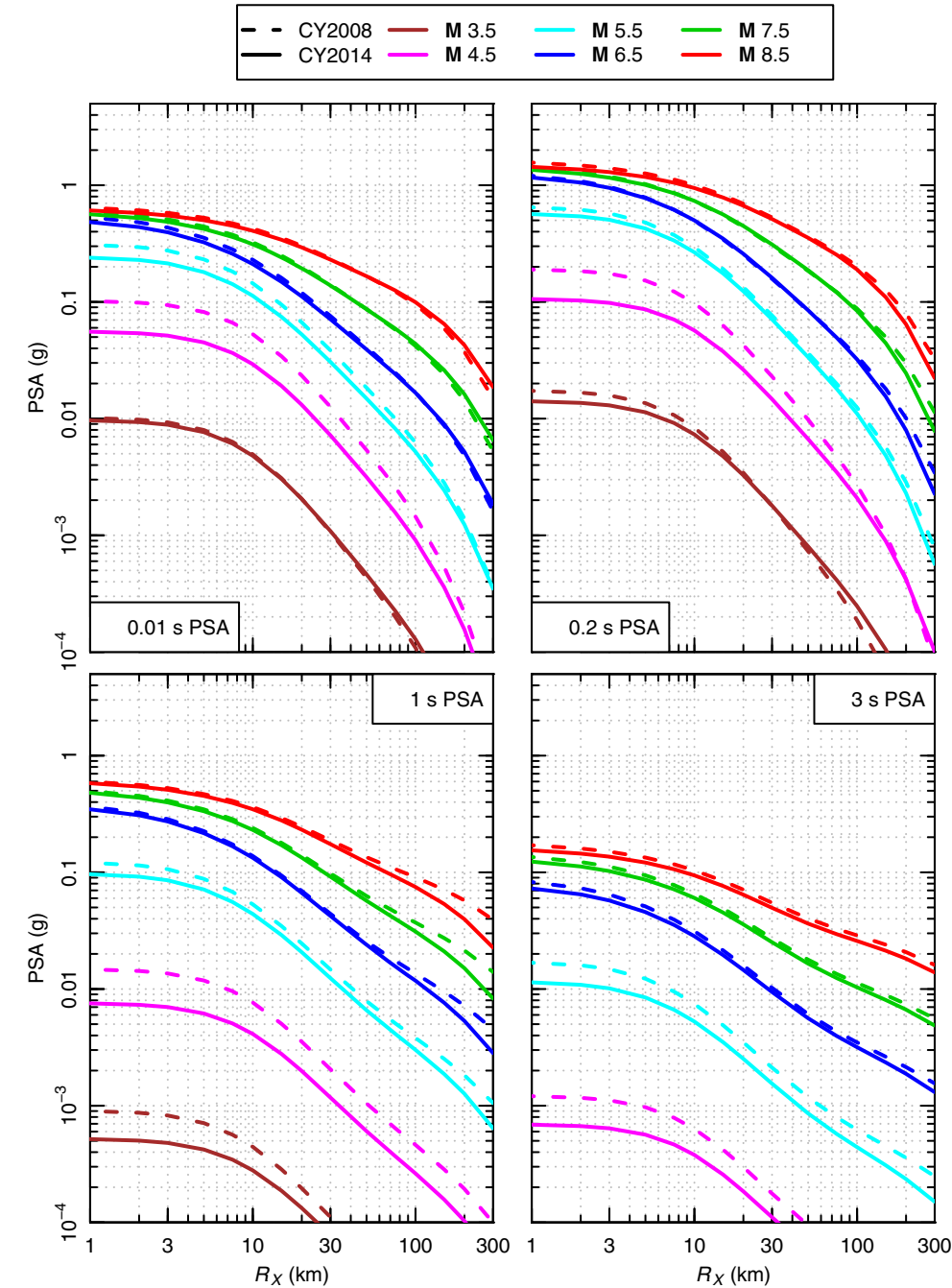


Figure 13. Continued.

NGA-West2 database in sufficient quantity to allow us to reliably estimate this effect, and it was thus not included in the updated model. However, users should consider such effects if the model is applied to sites with  $V_{S30}$  greater than 1,500 m/s.

The updated GMPE was developed using recordings from earthquakes with a maximum  $Z_{TOR}$  of 20 km. Furthermore, the  $Z_{TOR}$  and  $\mathbf{M}$  data suggest that the applicable range of



**Figure 14.** Median amplitude versus  $R_X$  predicted by the 2008 Chiou and Youngs NGA model (CY2008) and the updated model (CY2014) for vertical strike slip earthquake,  $V_{S30} = 760$  m/s average  $Z_{TOR}$  ( $\Delta Z_{TOR} = 0$ ), and  $\Delta DPP = 0$ .

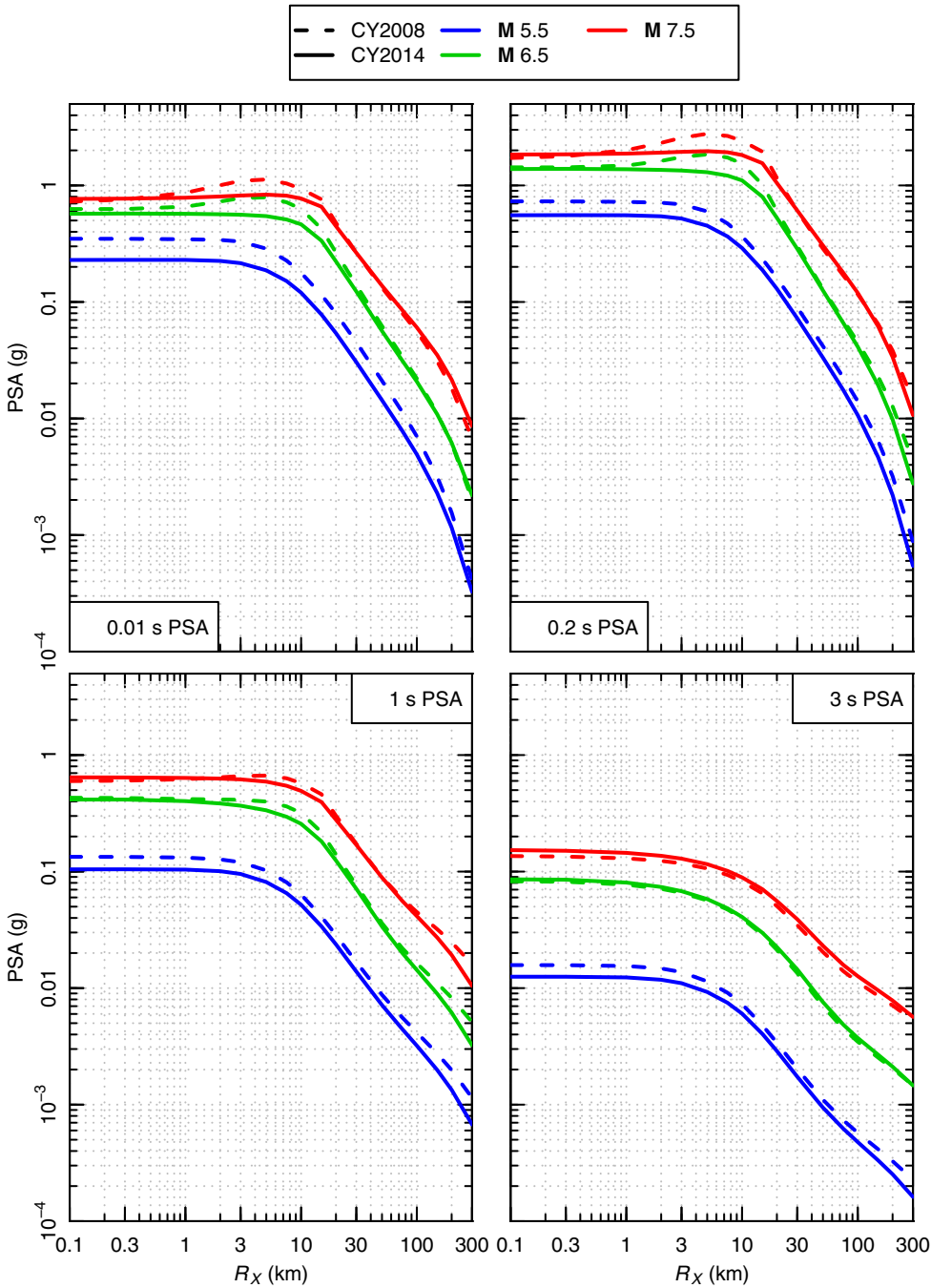


**Figure 15.** Median amplitude versus  $R_X$  predicted by the 2008 Chiou and Youngs NGA model (CY2008) and the updated model (CY2014) for reverse earthquake of 45° dip. Predictions are for average  $Z_{TOR}$  ( $\Delta Z_{TOR} = 0$ ),  $V_{S30} = 760$  m/s,  $\Delta DPP = 0$ , and for sites on the hanging wall ( $R_{JB} = 0$ ).

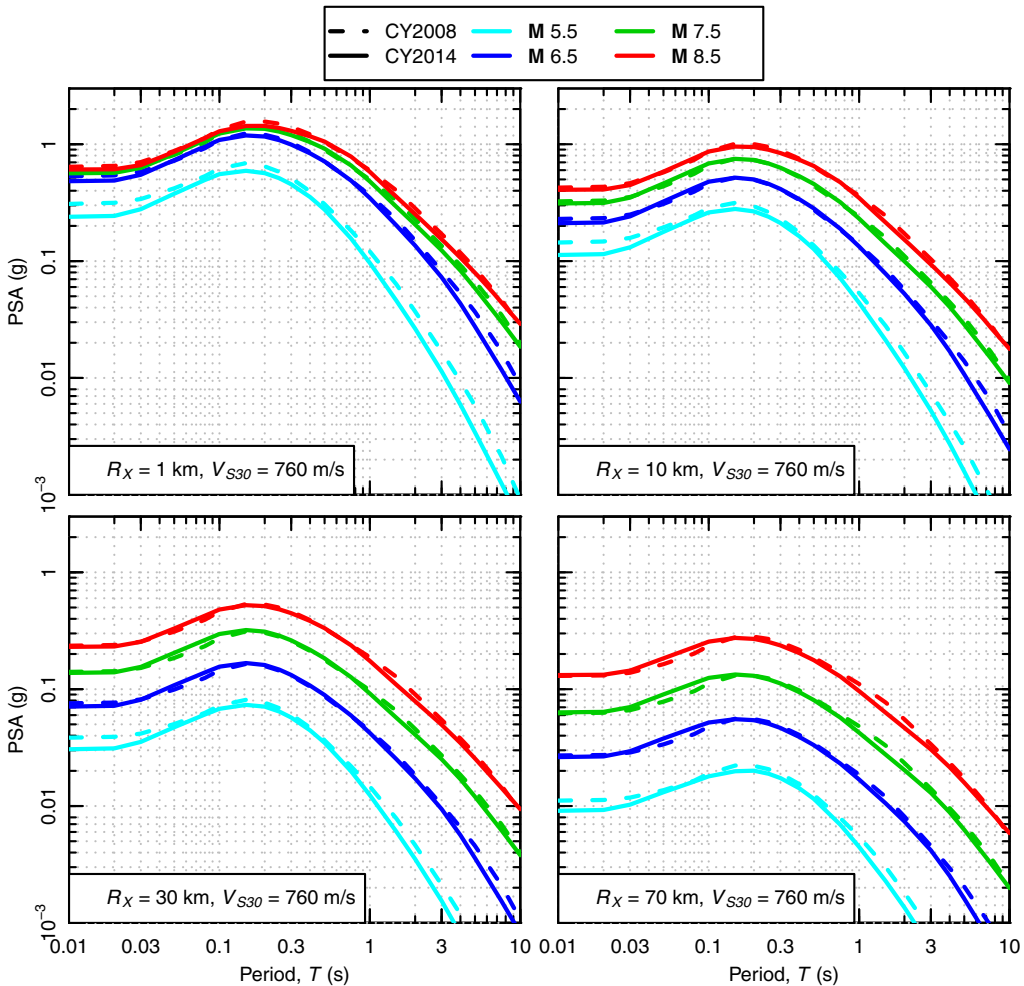


**Figure 16.** Median response spectra predicted by the 2008 Chiou and Youngs NGA model (CY2008) and the updated model (CY2014). Predictions are for vertical strike-slip earthquakes and  $V_{S30} = 760$  m/s.

$Z_{TOR}$  should be narrowing with increasing  $M$ . We do not recommend using large  $Z_{TOR}$  value for  $M > 7$  earthquakes beyond what was represented in the NGA-West2 database.

The majority of  $Z_{1.0}$  data used in our GMPE development were obtained from three-dimensional (3-D) velocity models for Southern California, the San Francisco Bay Area, and Japan. When applying our GMPE to these three regions, the same 3-D velocity models should be used to obtain site  $Z_{1.0}$ . Information on accessing these 3-D models is provided in [Ancheta et al. \(2013\)](#). For application to a site not covered by these velocity models and without other information to determine the site  $Z_{1.0}$ , we recommend using  $\Delta Z_{1.0} = 0$ . When applying our GMPE to a site whose  $Z_{1.0}$  is much smaller than the average

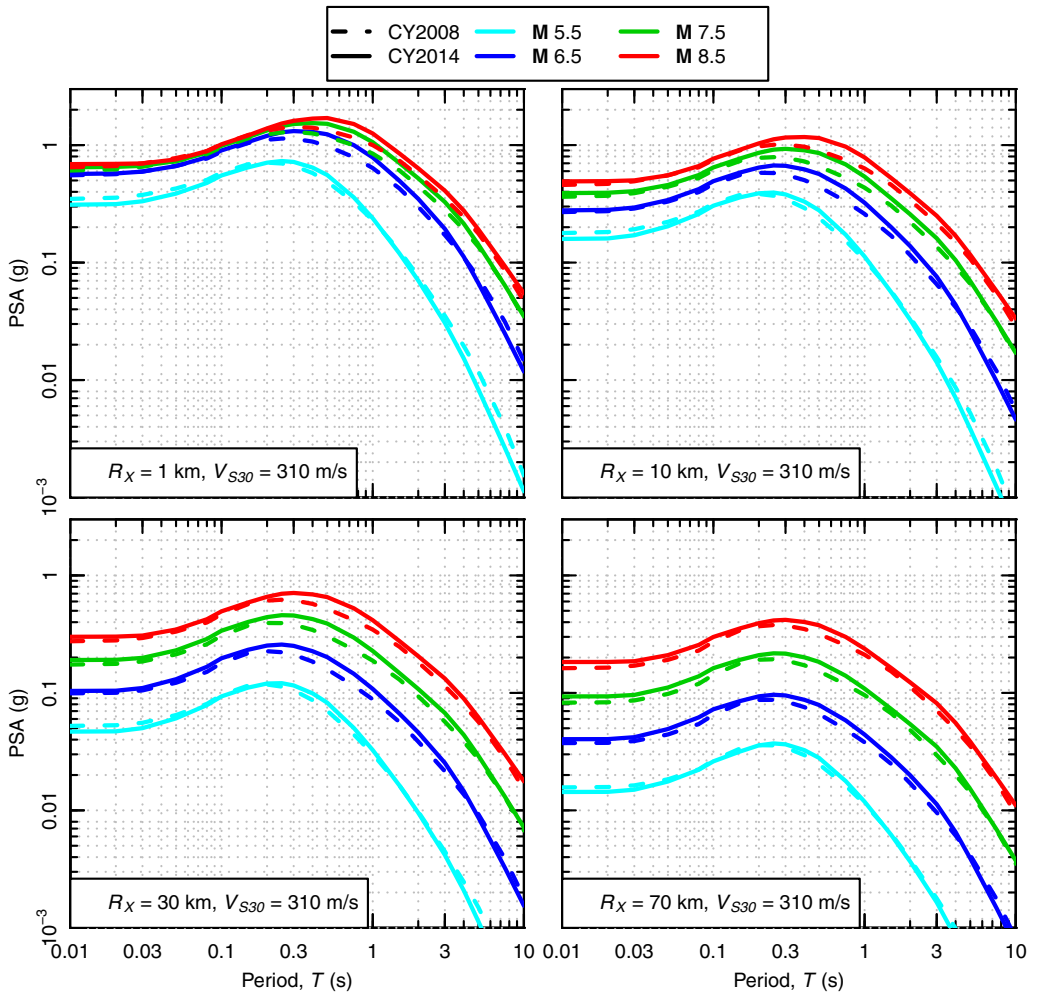


**Figure 17.** Median response spectra predicted by the 2008 Chiou and Youngs NGA model (CY2008) and the updated model (CY2014). Predictions are for vertical strike-slip earthquakes and  $V_{S30} = 310$  m/s.

$Z_{1,0}$  (a large negative  $\Delta Z_{1,0}$ ), the predicted motions should be checked to ensure that they are not lower than the predictions for reference condition of  $V_{S30} = 1,130$  m/s.

### ACKNOWLEDGEMENTS

This study was sponsored by the Pacific Earthquake Engineering Research Center (PEER) and funded by the California Earthquake Authority, the California Department of Transportation, and the Pacific Gas & Electric Company. Any opinions, findings, and conclusions or recommendations expressed in this material are those of the authors and do not necessarily reflect those of the sponsoring agencies. The authors wish to thank all

of the members of the PEER-NGA project for many enlightening interactions. We also thank Julian Bommer, James Kaklamanos, and an anonymous reviewer for their thoughtful review of this manuscript. The analysis and graphics in this paper were prepared using R (R Development Core Team 2014).

## REFERENCES

- Abrahamson, N. A., and Silva, W. J., 2008. Summary of the Abrahamson and Silva NGA ground motion relations, *Earthquake Spectra* **24**, 67–97.
- Al Atik, L., Abrahamson, N., Bommer, J. J., Scherbaum, F., Cotton, F., and Kuehn, N., 2010. The variability of ground motion prediction models and its components, *Seismological Research Letters* **81**, 794–801.
- Ancheta, T. D., Darragh, R. B., Stewart, J. P., Seyhan, E., Silva, W. J., Chiou, B. S.-J., Wooddell, K. E., Graves, R. W., Kottke, A. R., Boore, D. M., Kishida, T., and Donahue, J. L., 2013. *PEER NGA-West2 Database*, PEER Report 2013/03, Pacific Earthquake Engineering Research Center, University of California, Berkeley, CA.
- Boatwright, J., 2007. The persistence of directivity in small earthquakes, *Bull. Seismol. Soc. Am.* **97**, 1850–1861.
- Bozorgnia, Y., Abrahamson, N. A., Al Atik, L., Ancheta, T. D., Atkinson, G. M., Baker, J. W., Baltay, A., Boore, D. M., Campbell, K. W., Chiou, B. S.-J., Darragh, R., Day, S., Donahue, J., Graves, R. W., Gregor, N., Hanks, T., Idriss, I. M., Kamai, R., Kishida, T., Kottke, A., Mahin, S. A., Rezaeian, S., Rowshandel, B., Seyhan, E., Shahi, S., Shantz, T., Silva, W., Spudich, P., Stewart, J. P., Watson-Lamprey, J., Wooddell, K., and Youngs, R., 2014. NGA-West2 research project, *Earthquake Spectra* **30**, 973–987.
- Bragato, P. L., 2004. Regression analysis with truncated samples and its application to ground motion attenuation studies, *Bull. Seismol. Soc. Am.* **94**, 1369–1378.
- Campbell, K., 2003. Prediction of strong ground motion using the hybrid empirical method and its use in the development of ground motion (attenuation) relations in eastern North America, *Bull. Seismol. Soc. Am.* **93**, 1012–1033.
- Chiou, B. S.-J., Darragh, R., Gregor, N., and Silva, W., 2008. NGA project strong-motion database, *Earthquake Spectra* **24**, 23–44.
- Chiou, B. S.-J., and Youngs, R. R., 2008a. An NGA model for the average horizontal component of peak ground motion and response spectra, *Earthquake Spectra* **24**, 173–215.
- Chiou, B. S.-J., and Youngs, R. R., 2008b. *NGA Model for the Average Horizontal Component of Peak Ground Motion and Response Spectra*, PEER Report 2008/10, Pacific Earthquake Engineering Research Center, University of California, Berkeley, CA.
- Chiou, B. S.-J., and Youngs, R. R., 2012. Updating the Chiou and Youngs NGA model: regionalization of anelastic attenuation, in *Proceedings, 15th World Conference on Earthquake Engineering*, Lisbon, Portugal.
- Chiou, B. S.-J., and Youngs, R. R., 2013. *Update of the Chiou and Youngs NGA Ground Motion Model for Average Horizontal Component of Peak Ground Motion and Response Spectra*, PEER Report 2013/07, Pacific Earthquake Engineering Research Center, University of California, Berkeley, CA.
- Chiou, B. S.-J., Youngs, R. R., Abrahamson, N. A., and Addo, K., 2010. Ground motion attenuation model for small-to-moderate shallow crustal earthquakes in California and its implications on regionalization of ground motion prediction models, *Earthquake Spectra* **26**, 907–926.

- Cleveland, W. S., Grosse, E., and Shyu, W. M., 1993. Local regression models, Chapter 8, *Statistical Models in S*, J. M. Chambers and T. J. Hastie (eds.), Wadsworth & Brooks/Cole, 624 pp.
- Donahue, J. L., and Abrahamson, N. A., 2014. Simulation-based hanging wall effects, *Earthquake Spectra* **30**, 1269–1284.
- Kaklamanos, J., Baise, L. G., and Boore, D. M., 2011. Estimating unknown input parameters when implementing the NGA ground motion prediction equations in engineering practice, *Earthquake Spectra* **27**, 1219–1235.
- R Development Core Team, 2014. R: A language and environment for statistical computing, R Foundation for Statistical Computing, Vienna, Austria, available at <http://www.R-project.org>.
- Spudich, P., Bayless, J. R., Baker, J. W., Chiou, B. S.-J., Rowshandel, B., Shahi, S. K., and Somerville, P., 2013. *Final Report of the NGA-West2 Directivity Working Group*, PEER Report No. 2013/09, Pacific Earthquake Engineering Research Center, University of California, Berkeley, 129 pp.
- Spudich, P., and Chiou, B. S.-J., 2008. Directivity in NGA earthquake ground motions: analysis using isochrone theory, *Earthquake Spectra* **24**, 279–298.
- Toro, G. R., 1981. Biases in Seismic Ground Motion Prediction, Ph.D. Thesis, Department of Civil Engineering, Massachusetts Institute of Technology, 133 pp.
- Wooddell, K. E., and Abrahamson, N. A., 2014. Classification of main shocks and aftershocks in the NGA-West2 database, *Earthquake Spectra* **30**, 1257–1267.

(Received 28 July 2013; accepted 2 March 2014)